6816–6824 Nucleic Acids Research, 2008, Vol. 36, No. 21 Published online 25 October 2008
doi:10.1093/nar/gkn767

Elucidation of the mode of interaction in the UP1–telomerase RNA–telomeric DNA ternary complex which serves to recruit telomerase to telomeric DNA and to enhance the telomerase activity

Takashi Nagata[1], Yusuke Takada[1], Asami Ono[2], Kayoko Nagata[2], Yuki Konishi[2], Takeshi Nukina[2], Manami Ono[1], Akimasa Matsugami[1], Ayako Furukawa[1], Natsuki Fujimoto[1], Hirokazu Fukuda[3], Hitoshi Nakagama[3] and Masato Katahira[1,4,*]

[1]Supramolecular Biology, International Graduate School of Arts and Sciences, Yokohama City University, 1-7-29 Suehiro-cho, Tsurumi-ku, Yokohama 230-0045, [2]Department of Environment and Natural Sciences, Graduate School of Environment and Information Sciences, Yokohama National University, 79–7 Tokiwadai, Hodogaya-ku, Yokohama 240-8501, [3]Biochemistry Division, National Cancer Center Research Institute, 5-1-1 Tsukiji, Chuo-ku, Tokyo 104-0045 and [4]PRESTO, JST, Japan

Received August 6, 2008; Revised and Accepted October 7, 2008

ABSTRACT

We found that UP1, a proteolytic product of heterogeneous nuclear ribonucleoprotein A1 (hnRNP A1), both enhances and represses the telomerase activity. The formation of the UP1–telomerase RNA–telomeric DNA ternary complex was revealed by a gel retardation experiment. The interactions in the ternary and binary complexes were elucidated by NMR. UP1 has two nucleic acid-binding domains, BD1 and BD2. In the UP1–telomerase RNA binary complex, both BD1 and BD2 interact with telomerase RNA. Interestingly, when telomeric DNA was added to the binary complex, telomeric DNA bound to BD1 in place of telomerase RNA. Thus, BD1 basically binds to telomeric DNA, while BD2 mainly binds to telomerase RNA, which resulted in the formation of the ternary complex. Here, UP1 bridges telomerase and telomeric DNA. It is supposed that UP1/hnRNP A1 serves to recruit telomerase to telomeric DNA through the formation of the ternary complex. A model has been proposed for how hnRNP A1/UP1 contributes to enhancement of the telomerase activity through recruitment and unfolding of the quadruplex of telomeric DNA.

INTRODUCTION

Highly repetitive sequences called telomeres exist at the ends of eukaryotic chromosomes. Human telomeric DNA is 5- to 8-kb long and composed of repeats of the d(TTAGGG) sequence, with a 3′-single-stranded overhang of ~200 nt (1,2). Telomeres are associated with a specific set of proteins that serve to protect chromosome ends from fusion and degradation (3–5). In mammals, TRF2 binds to double-stranded telomeric DNA and protects the telomere ends (6). Another protein, POT1, is thought to modulate telomere elongation (7–9). The T-loop structure, in which the overhang loops back and invades the duplex telomeric DNA, can also protect chromosome ends (10).

The telomeres of most somatic cells become shorter on replication; whereas, those of germ cells and cancer cells maintain their lengths through elongation by telomerase, which is active in these cells (11). Telomerase is composed of reverse transcriptase (TERT) and telomerase RNA, which is used as a template for reverse transcription. It is unknown how telomerase is recruited to telomeres. Telomerase requires an accessible 3′-overhang for the elongation. DNA rich in guanosine residues tends to form a quadruplex with guanine-tetrad planes as core structures (12). Telomeric DNA is rich in guanosine residues and thus its quadruplex structure is supposed to play certain roles in the regulation of telomere length. In particular, the finding that telomerase activity is inhibited on formation of the quadruplex (13–15) has attracted attention in terms of the development of novel anticancer drugs.

Heterogeneous nuclear ribonucleoprotein A1 (hnRNP A1) is one of the most abundant nuclear proteins and involved in a variety of processes such as alternative splicing and mRNA transport (16–20). HnRNP A1 is composed of 320 residues. UP1 is a proteolytic product of hnRNP A1 and encompasses the N-terminal two-thirds

*To whom correspondence should be addressed. Tel: +81 45 508 7213; Fax: +81 45 508 7361; Email: katahira@tsurumi.yokohama-cu.ac.jp

of hnRNP A1, being composed of 196 residues. HnRNP A1 and UP1 possess two ribonucleoprotein (RNP)-type DNA/RNA-binding domains (BD1: K15-A89 and BD2: K106–A180). It has been shown that a deficiency of hnRNP A1 expression in a mouse erythroleukemic cell line is associated with short telomeres and that restoring hnRNP A1 expression increases the length of telomeres. Telomere elongation was also observed upon the introduction of exogenous UP1 (21). It was found that RNAi-induced reduction in hnRNP A1/A2 in HeLa cells was associated with a change in the distribution of the length of G-tails (22). Then, it was reported that hnRNP A1 stimulates telomerase activity. The association of hnRNP A1 with telomeres *in vivo* was also reported (23). A mechanism by which hnRNP A1/UP1 stimulates telomerase activity and modulates telomere length has been proposed. We demonstrated that UP1 can unfold the quadruplex structure of telomeric DNA into a single-stranded structure (24), which was later supported by another group (25). Here, UP1 may either directly unfold the quadruplex into the single-stranded structure or indirectly shift the equilibrium to the single-stranded structure through binding and stabilization of the single-stranded structure. We also revealed that DNA synthesis is arrested at the G-rich region of the synthetic template in a specific DNA polymerase stop assay due to the formation of the quadruplex and that UP1 can abrogate the arrest through unfolding of the quadruplex (24). Through the analogy, this finding led us to propose that hnRNP A1/UP1 facilitate telomerase activity through unfolding of the quadruplex of the overhang, which results in the provision of an accessible overhang (24). A similar role and mechanism in telomere maintenance were proposed for another related protein, hnRNP D, on the basis of its structure and ability to unfold the quadruplex (26). Later, a related idea was proposed by another group (23).

Another mechanism was also proposed. It was found that hnRNP A1 may interact simultaneously with telomerase RNA and telomeric DNA. It was suggested that hnRNP A1 may help recruit telomerase to the ends of chromosomes through the simultaneous interaction, resulting in the enhancement of the telomerase activity (27). Stimulated by this proposal, we started the present study. First, we found that UP1 both enhances and represses the synthesis of telomeric DNA, depending on the length of newly synthesized telomeric DNA. The formation of the UP1–telomerase RNA–telomeric DNA ternary complex was revealed by a gel retardation experiment. Then, the interactions in the binary and ternary complexes were elucidated for the first time at the residue level by NMR. On the basis of the elucidated interactions, a model accounting for the enhancement and repression of the telomerase activity by UP1 was constructed.

MATERIALS AND METHODS

Preparation of UP1

The expression plasmid pGEX-6P-2 was described previously (24). *Escherichia coli*, BL21(DE3), was transformed with this plasmid. The cells were grown in LB medium and GST-UP1 fusion protein was expressed. For the preparation of ^{13}C, ^{15}N-labelled UP1, the LB medium was replaced by M9 minimal medium containing $^{15}NH_4Cl$ and ^{13}C-glucose. GST-UP1 was purified with a glutathione Sepharose FF column (GE Healthcare, Buckinghamshire, England). Release of UP1 from GST-UP1 was performed with PreScission Protease (GE Healthcare). UP1 was further purified with a Q Sepharose FF column (GE Healthcare).

Assaying of the telomerase activity

A telomerase extract was prepared from HeLa cells in lysis buffer (11). The presence of either hnRNP A1 or hnRNP D was monitored by western blotting. Telomerase activity was examined by means of a modified TRAP method (28) with TeloChaser (Toyobo, Osaka, Japan). Products were run on a 10% polyacrylamide gel, stained with SYBER Green II, and detected with a FLA 5000 (Fuji Film, Tokyo, Japan). The intensities of bands were quantified with Image J.

Gel retardation experiments

Cy5-labelled 15-mer telomerase RNA, r(UGAGAAGGGC GUAGG), was incubated with various amounts of UP1 at 4°C for 30 min in a 20 µl solution comprising 10 mM Tris (pH 7.5), 50 mM NaCl, 1 mM EDTA, 5% glycerol and 2 µg BSA. Competitor tRNA was also added in some case. For the examination of the formation of the ternary complex, 12-mer telomeric DNA, d(GTCTTAGGGCAG), was added to the solution of the UP1:15-mer telomerase RNA binary complex. DNA possessing one telomeric repeat in the middle of a non-telomeric sequence was used, because DNA with multiple telomeric repeats sometimes could form the artificial aggregate caused by intra- and intermolecular interactions through multiple interactive sites. The mixtures were run on a 10% polyacrylamide gel, with detection with a FLA2000 (Fuji Film).

NMR spectroscopy

UP1 was dissolved in a solution comprising 20 mM Na-phosphate buffer (pH 6.5), either 0 or 150 mM NaCl, 2.7 mM ^2H-DTT, 1 mM protease inhibitors, Pefabloc SC(AEBSF) (Roche Applied Science, Mannheim, Germany) and 5% ^2H_2O. The UP1 concentrations were 0.5–1.0 mM for the structural analysis and 0.2 mM for the titration. NMR spectra were recorded with Bruker (Rheinstetten, Germany) DRX600 and DRX800 spectrometers equipped with a cryoprobe. The following NMR spectra were obtained to assign resonances: HSQC, ^{15}N-edited NOESY-HSQC, ^{13}C-edited NOESY-HSQC, HNCA, HN(CO)CA, HNCO, HN(CA)CO, HNCACB, CBCA (CO)NH, C(CO)NH and H(CCO)NH. For the titration experiments as to the formation of binary complexes, a concentrated solution of either 15-mer telomerase RNA or 12-mer telomeric DNA was added step by step to the UP1 solution. For the titration experiment as to the formation of the ternary complex, a concentrated solution of 12-mer telomeric DNA was added step by step to the solution of UP1–telomerase RNA binary complex. An equimolar amount of telomeric DNA to telomerase RNA was added at the end of the titration. Spectra were

processed and analyzed with XWIN-NMR (Bruker), NMRPipe (29), Capp/Pipp/Stapp (30), Sparky (31) and Kujira (32). Combined chemical shift perturbation as to H^N and N was defined and calculated as

$$[(\Delta\delta_{NH}*600)^2 + (\Delta\delta_N*60*2)^2]^{1/2}$$

where $\Delta\delta_{HN}$ and $\Delta\delta_N$ are the chemical shift perturbations for H^N and N resonances, respectively.

RESULTS

Effect of UP1 on the telomerase activity

The effect of UP1 on the telomerase activity was examined. Before the examination, it was revealed on western blotting that hnRNP A1 and hnRNP D were almost completely depleted in the course of the preparation of the telomerase extract from HeLa cells, although the HeLa cells originally contained these proteins (data not shown). It is supposed that endogenous hnRNP A1 and hnRNP D bound to endogenous DNA/RNA and were co-precipitated during the preparation, resulting in the depletion. Then, Figure 1 shows the effect of UP1 on the telomerase activity of the extract prepared from HeLa cells, as monitored with a modified TRAP method. The intensities of all bands were summed up for each lane in Figure 1. The total intensity in each lane was calibrated with the intensity of the band of the internal control. The calibrated total intensities in individual lanes were compared. The relative intensities were 1.0, 1.7, 1.3 and 1.0 for the UP1 concentrations of 0 μM, 1 μM, 2.5 μM and 5 μM, respectively. Thus, UP1 increases the total activity of telomerase. The primer used in a modified TRAP method contains three d(GGGG) sequences and one d(GG) sequence (28), and so potentially may form a quadruplex. When telomeric DNA repeats are added to the primer by telomerase, the formation of the quadruplex is more likely. It is supposed that the enhancement of the activity is brought about by UP1 through recruitment of telomerase to telomeric DNA and also through unfolding of the quadruplex of telomeric DNA, as discussed later. The enhancement became the maximum with the UP1 concentration of ~1 μM and was counteracted with higher UP1 concentrations. UP1 is denatured and removed from a system before a PCR step in the procedure with a TeloChaser. Therefore, it is certain that the affect of UP1 on the TRAP assay is at the level of extension by telomerase and not PCR amplification.

It should be noted that the intensities of bands corresponding to relatively short DNA increase on the addition of UP1, while those corresponding to relatively long DNA decrease. For example, when the intensities with 1 μM UP1 (lane 3) are compared with those with no UP1 (lane 2), an increase is observed for bands corresponding to less than ~160 bp, while a decrease is observed for those corresponding to more than ~160 bp.

Enhancement of the telomerase activity by hnRNP A1/UP1 was reported by another group (23). They did not report that the enhancement becomes maximum at a certain hnRNP A1/UP1 concentration and that it is counteracted with higher hnRNP A1/UP1 concentrations. Thus, our results are consistent with their report and provide a more comprehensive view as to the effect of hnRNP A1/UP1 on the telomerase activity. In fact, it was reported by other group that binding of hnRNP A1/UP1 to single-stranded telomeric repeats inhibits telomerase extension (33). The apparent discrepancy may be rationalized to some extent by taking into account the hnRNP A1/UP1 concentrations applied to each experiment.

It was not reported either that the effect of hnRNP A1/UP1 depends on the length of synthesized telomeric DNA, because the synthesis of relatively short telomeric DNA was examined previously (23). The interpretation of our findings will be discussed later.

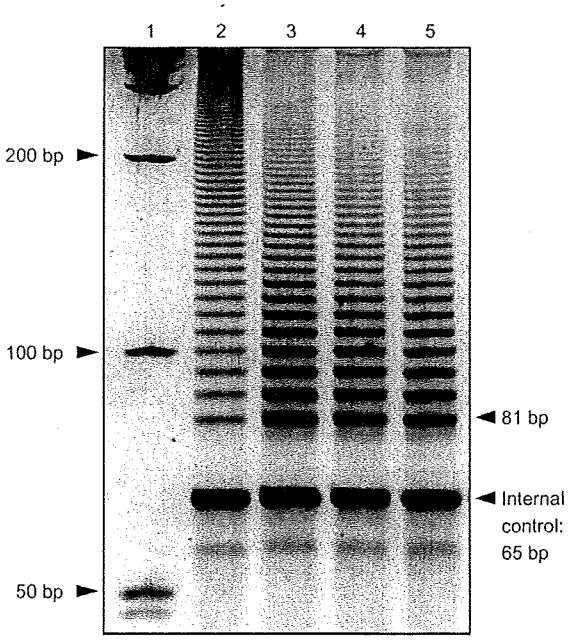

Figure 1. The effect of UP1 on the telomerase activity, as monitored by the TRAP method. The elongation of telomeric DNA was carried out with a telomerase extract prepared from HeLa cells with increasing amounts of UP1. Lane: 1, markers; 2, 5 μM, 0 μM, 1 μM, 2.5 μM and 5 μM UP1.

Formation of the UP1–telomerase RNA–telomeric DNA ternary complex revealed by a gel retardation experiment

It was shown that UP1 specifically binds to telomerase RNA (27). Analysis with a deletion mutant of telomerase RNA indicated that binding of UP1 is detected to the 5′-terminal 71 nt of telomerase RNA, while binding is not detected to the 5′-terminal 56 nt of telomerase RNA (27). This suggests that residues 56–71 of telomerase RNA may be the binding site for UP1. We examined if UP1 binds to 15-mer telomerase RNA, r(UGAGA AGGGCGUAGG), corresponding to residues 56–71 of telomerase RNA through a gel retardation experiment. Figure 2A shows that UP1 binds to the 15-mer. The binding is rather strong, the dissociation constant being estimated to be between 5×10^{-8} M and 5×10^{-7} M from Figure 2A. This is the first demonstration that the short fragment of telomerase RNA is bound by UP1.

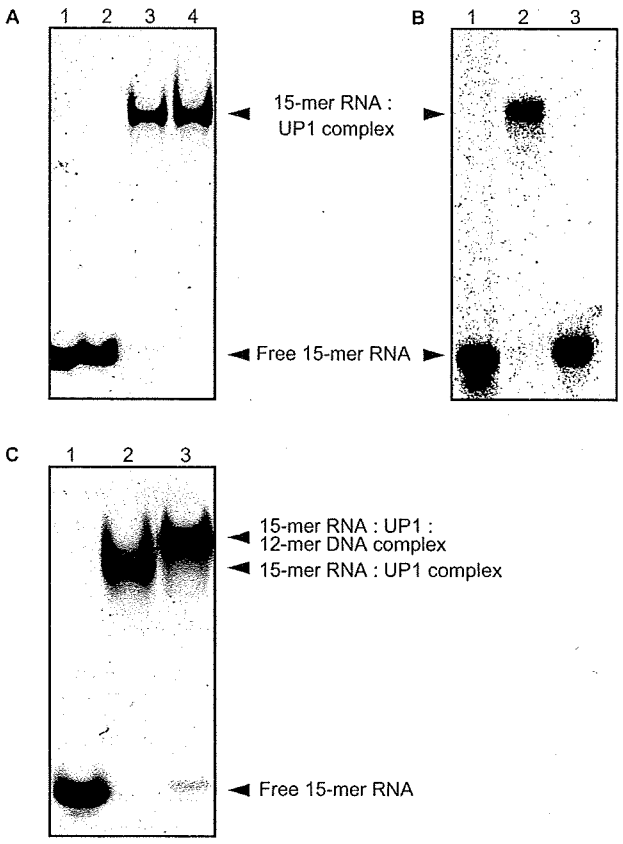

Figure 2. The formation of the binary and ternary complexes, as revealed by gel retardation experiments. (**A**) The binding of UP1 to 15-mer telomerase RNA. Cy5-labelled 15-mer telomerase RNA was incubated with increasing amounts of UP1, 0 μM, 0.05 μM, 0.5 μM and 1 μM for lanes 1–4. The mixtures were run on a polyacrylamide gel. (**B**) The binding of UP1 to 15-mer telomerase RNA in the presence of competitor tRNA. Cy5-labelled 15-mer telomerase RNA and UP1 (5 μM) were incubated in the presence of an excess amount of competitor tRNA. The weight ratios of tRNA/15-mer were 200 and 2000 for lanes 2 and 3, respectively. The 15-mer alone was applied for lane 1. (**C**) The formation of the UP1–telomerase RNA–telomeric DNA ternary complex. Cy5-labelled 15-mer telomerase RNA was incubated alone (lane 1) or with UP1 (5 μM) (lane 2). Then, 12-mer telomeric DNA (5 μM) was added to the solution of the UP1: 15-mer telomerase RNA binary complex (lane 3).

The dissociation constant of the UP1:full-length telomerase RNA complex was shown to be between 2.5×10^{-7} M and 5×10^{-7} M (26). Thus, the affinity of UP1 to 15-mer RNA is comparable to or even higher than that to the full-length RNA (27). It was shown that the binding of UP1 to full-length telomerase RNA is specific (27). Figure 2B shows that the addition of a 200-fold excess of tRNA as a competitor does not disrupt the binding of UP1 to the 15-mer (lane 2). This implies that the binding of UP1 to the 15-mer may also be specific like that to full-length telomerase RNA, which is expected from rather strong affinity of UP1 to the 15-mer.

When 12-mer DNA containing a telomeric DNA sequence, d(GTCTTAGGGCGA), was added to the UP1:15-mer telomerase RNA binary complex, a super-shift of the band which may correspond to the formation of the ternary complex was observed in the gel retardation experiment (lane 3 in Figure 2C). The results of western blotting confirmed that the super-shifted band still contains UP1 (data not shown). Therefore, the super shift strongly suggests the formation of the UP1:15-mer telomerase RNA:12-mer telomeric DNA ternary complex. The formation of the ternary complex was suggested on the basis of the results of affinity chromatography, in which longer telomerase RNA and DNA possessing multiple telomeric repeats were used (27). Our results on gel retardation are consistent with this idea.

Resonance assignments and the deduced secondary structure of UP1

The polypeptide produced on the cleavage of GST-UP1 with PreScission Protease is composed of the UP1 (M1-R196) protein and an N-terminal linker peptide (GPLGSPGIRCSV), totally 208 residues. Sequential assignments of the main chain H^N, N, C^α, C^β and C′ resonances were made for the peptide of 208 residues in the same way as reported for a related protein, hnRNP D (26,34,35). Resonance assignments were accomplished for ca. 90% of the polypeptide. The polypeptide corresponding to the N-terminal half of UP1 was analyzed and the assignments were reported (36). It was confirmed that our assignments for the whole UP1 are consistent with those reported for the N-terminal half.

The secondary structure of UP1 was deduced on the basis of the resonance assignments with the chemical shift index method (37). It was confirmed that the deduced secondary structure in solution is basically consistent with the structure found in a crystal (38–40).

Interactions in the UP1–telomerase RNA and UP1–telomeric DNA binary complexes revealed by NMR

The chemical shift perturbations of the ^1H-^{15}N HSQC correlation peaks of UP1 on the addition of 15-mer telomerase RNA were observed until a 1:1 molar ratio (data not shown). No further chemical shift perturbation was observed when further 15-mer was added. The increase in the line width of the correlation peak was moderate. These results indicate that one telomerase RNA molecule binds to one UP1 molecule. The chemical shift perturbations of the UP1 correlation peaks on the addition of telomerase RNA are mapped on the UP1 monomer structure of the dimer observed in a crystal (38–40). Most chemical shift perturbations are located on the two β-sheets side, and a few chemical shift perturbations on the back side (Figure 3A), which indicates that the two β-sheets side is the binding surface. The binding on the β-sheet side was observed for other RNP-type binding domains, including those of a related protein, hnRNP D (26,34,35).

It was suggested that BD2 of hnRNP A1/UP1 is responsible for binding to telomerase RNA (26). However, the chemical shift perturbations were observed not only for BD2 but also for BD1 of UP1 (Figure 3A). This indicates that both BDs bind to telomerase RNA to form the UP1–telomerase RNA binary complex under the conditions used for NMR experiments (Figure 3C).

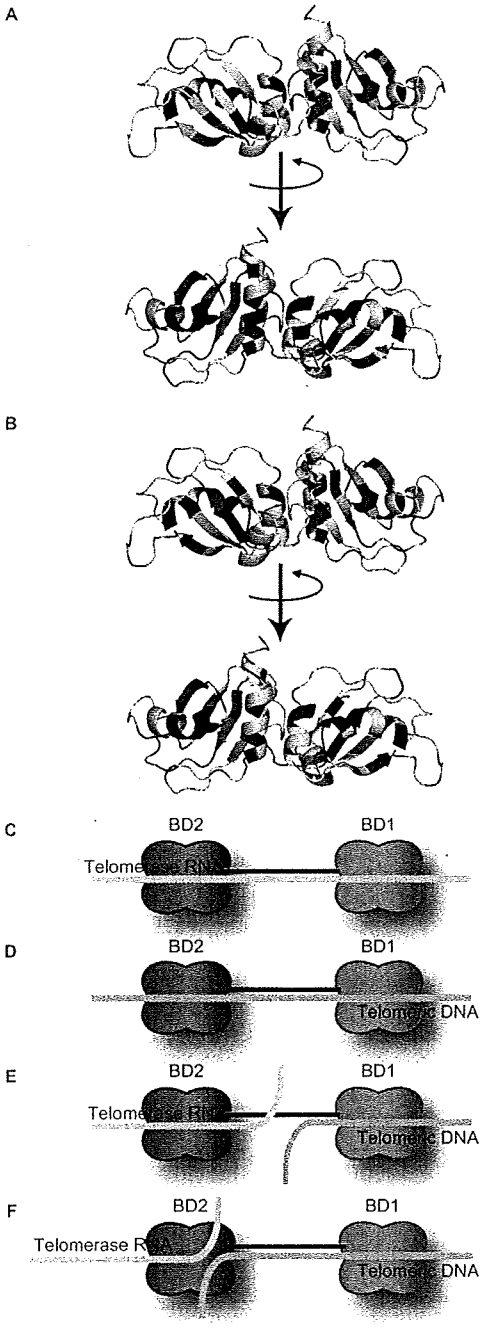

Figure 3. Summary of the interactions and the schematic representations of the binary and ternary complexes. Mapping of chemical shift perturbations upon binding of 15-mer telomerase RNA (**A**) and 12-mer telomeric DNA (**B**), respectively. The crystal structure of UP1 (PDB ID: 2up1) is used for mapping. The residues with combined chemical shift perturbations as to H^N and N of >75 Hz, 75–45 Hz and 45–0 Hz are colored red, yellow and black, respectively, and those whose ^1H-^{15}N correlation peak disappeared are colored blue. The residues whose chemical shift perturbations were not unambiguously determined due to overlapping of peaks are colored gray. Schematic representations of the UP1 telomerase RNA binary complex (**C**), the UP1 telomeric DNA binary complex (**D**), the UP1 telomerase RNA telomeric DNA ternary complex (**E**) and the more precise UP1 telomerase RNA telomeric DNA ternary complex (**F**).

The chemical shift perturbations mainly on the two β-sheets side were also observed when 12-mer telomeric DNA was added to the UP1 solution (Figure 3B). It was suggested that BD1 of hnRNP A1/UP1 is responsible for binding to telomeric DNA, although the possibility of the binding of BD2 to telomeric DNA was preserved (27). This time, the chemical shift perturbations were observed for both BDs of UP1, indicating that both BDs bind to telomeric DNA to form the UP1–telomeric DNA binary complex under the present conditions (Figure 3D).

The crystal structure of UP1 bound to the single-stranded telomeric repeat DNA was reported (40). In crystal, dimeric UP1 bound to two oligodeoxyribonucleotides. Judging from the narrow line widths of ^1H-^{15}N HSQC correlation peaks of either UP1–telomerase RNA or UP1–telomeric DNA binary complexes, it is supposed that UP1 is monomeric in both the complexes.

Interactions in the UP1–telomerase RNA–telomeric DNA ternary complex revealed by NMR

When 12-mer telomeric DNA was added to a solution of the UP1–telomerase RNA binary complex, interesting changes in the chemical shift perturbations were observed. The position of an HSQC correlation peak of a certain residue for the UP1–telomerase RNA binary complex (green) is generally different from that for the UP1–telomeric DNA binary complex (black), as shown in Figure 4. For most residues of BD1, when an equimolar amount of telomeric DNA to telomerase RNA was added to the UP1–telomerase RNA binary complex, the correlation peak originally observed at the position for the UP1–telomerase RNA binary complex appeared at the position for the UP1–telomeric DNA binary complex (Figure 4A–C). This indicates that a portion of telomerase RNA originally bound to BD1 dissociated and that telomeric DNA bound to BD1 in place of telomerase RNA (Figure 3E). Although a weak correlation peak remains at the position for the UP1–telomerase RNA binary complex for some residues of BD1, a dominant stronger correlation peak nonetheless appears at the position for the UP1–telomeric DNA binary complex (Figure 4D and E). This once again reveals that BD1 is basically bound by telomeric DNA in the ternary complex.

hnRNP A2 also has two DNA/RNA-binding domains, BD1 and BD2. DNA/RNA binding of hnRNP A2 was characterized, and the possibility was raised that telomeric DNA may compete with telomerase RNA for binding to BD1 of hnRNP A2 (41). This is actually what we experimentally found for BD1 of hnRNP A1. Thus, hnRNP A1 and hnRNP A2 may share some features on DNA/RNA binding, although they exhibit differences in other aspects (41).

For many residues of BD2, in contrast, a correlation peak remains at the position for the UP1–telomerase RNA binary complex even after the addition of telomeric DNA (Figure 4F and G). This indicates that the portion of telomerase RNA originally bound to BD2 remains there (Figure 3E). In summary, analysis of chemical shift perturbations revealed the formation of the UP1–telomerase RNA–telomeric DNA ternary complex in which BD1

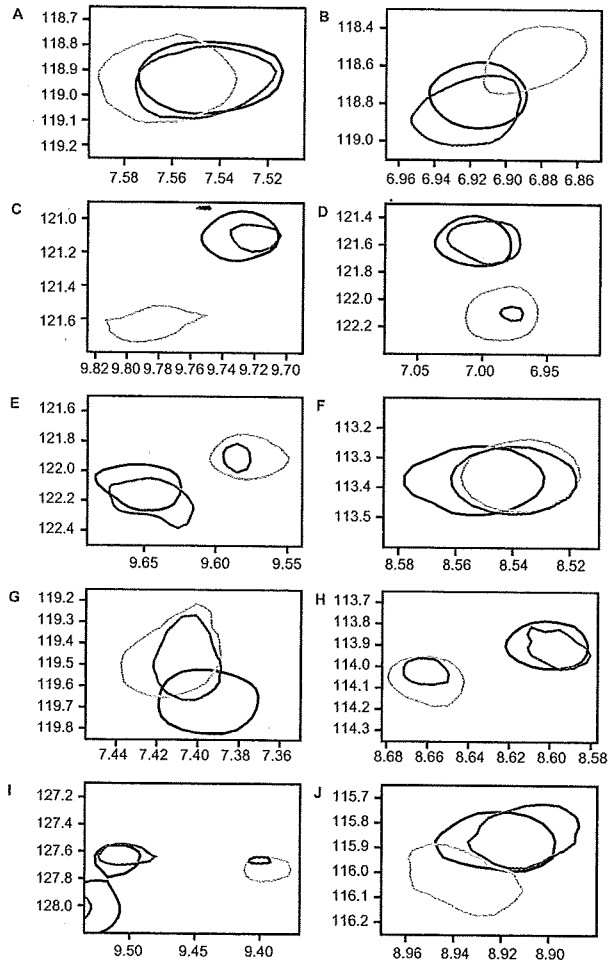

Figure 4. The formation of the ternary complex, as revealed by NMR chemical shift perturbations. Comparison of the position of a ^{1}H-^{15}N correlation peak for the UP1–telomerase RNA–telomeric DNA ternary complex (red) with those for either the UP1–telomerase RNA binary complex (green) or the UP1–telomeric DNA binary complex (black). The ternary complex was made by the titration of telomeric DNA to the UP1 telomerase RNA binary complex. An equimolar amount of telomeric DNA to telomerase RNA was added to the binary complex at the end of the titration. (A–E): D42, V68, K87, A74 and H77 of BD1, respectively; (F–J): H119, I162, F150, F153 and I107 of BD2, respectively.

and BD2 bind to telomeric DNA and telomerase RNA, respectively (Figure 3E).

It was noticed that for some residues of BD2, a dominant correlation peak appears at the position for the UP1–telomeric DNA binary complex, although a weak correlation peak remains at the position for the UP1–telomerase RNA binary complex (Figure 4H and I). There is even a case that a correlation peak of a residue of BD2 appears at the position for the UP1–telomeric DNA binary complex, exclusively (Figure 4J). These results imply that a portion of telomerase RNA originally bound to BD2 also dissociated to some extent and that telomeric DNA bound to BD2 in place of telomerase RNA in the ternary complex (Figure 3F).

DISCUSSION

We demonstrated that UP1 enhances the synthesis of relatively short telomeric DNA by telomerase. We revealed the formation of the UP1–telomerase RNA–telomeric DNA ternary complex through a gel retardation experiment, which is consistent with the previous suggestion derived from the experiment involving affinity chromatography (27). NMR chemical shift perturbation analysis provided detailed views of the interactions in the ternary complex, together with those in the UP1–telomerase RNA and UP1–telomeric DNA binary complexes. On the basis of the obtained information, we propose a model of how UP1 enhances the telomerase activity. First, UP1 captures telomerase through the interaction of both the BDs with telomerase RNA (Figure 5A), as revealed by NMR chemical shift perturbation analysis (Figure 3A and C). It is supposed that the presence of TERT bound to telomerase RNA does not interfere with the UP1–telomerase RNA interaction. In fact, it was shown that a column carrying GST-UP1 can specifically recover telomerase activity from a cell extract (21). At least 20% of total telomerase activity was present in the UP1-bound fraction (21). Then, telomerase-bound UP1 effectively searches for telomeric DNA with its affinity to telomeric DNA, particularly with the affinity of BD1 to telomeric DNA. When telomerase-bound UP1 encounters telomeric DNA, the BDs of UP1, particularly BD1, unfold the quadruplex structure of telomeric DNA into a single-stranded structure. Then, the UP1–telomerase–telomeric DNA ternary complex is formed through the interaction of BD1 with telomeric DNA (Figure 5B), as NMR indicated that telomeric DNA bound to BD1 in place of telomerase RNA (Figures 3E, F and 4). UP1 bridges telomerase and telomeric DNA through simultaneous BD1–telomeric DNA and BD2–telomerase RNA interactions. In this way, UP1 serves to recruit telomerase to telomeric DNA. Thus, telomerase is brought to telomeric DNA where it should function. Finally, telomerase RNA associates with telomeric DNA using the complementarity to telomeric DNA, which is present at the edge of the template region of telomerase RNA, and TERT synthesizes new telomeric DNA, UP1 being released meanwhile (Figure 5C). In this model, the enhancement of the telomerase activity is brought about through the recruitment of telomerase to telomeric DNA and the unfolding of the quadruplex structure of telomeric DNA into a single-stranded structure by UP1.

It was proposed that POT1 protein may disrupt quadruplex structures in telomeric DNA and thereby allow proper elongation by telomerase (42). So, hnRNP A1/UP1 and POT1 may share the similar role in telomere maintenance, at least in terms of unfolding. Therefore, the unfolding may be performed by POT1, in place of hnRNP A1/UP1, in some cases.

When the UP1 concentration was raised to 2.5 μM, the beginning of the decrease in the total telomerase activity was observed (Figure 1). Occupation of the 3′-overhang of telomeric DNA by an excess amount of UP1 and resultant interference with binding of telomerase to telomeric DNA may account for this phenomenon (Figure 5D).

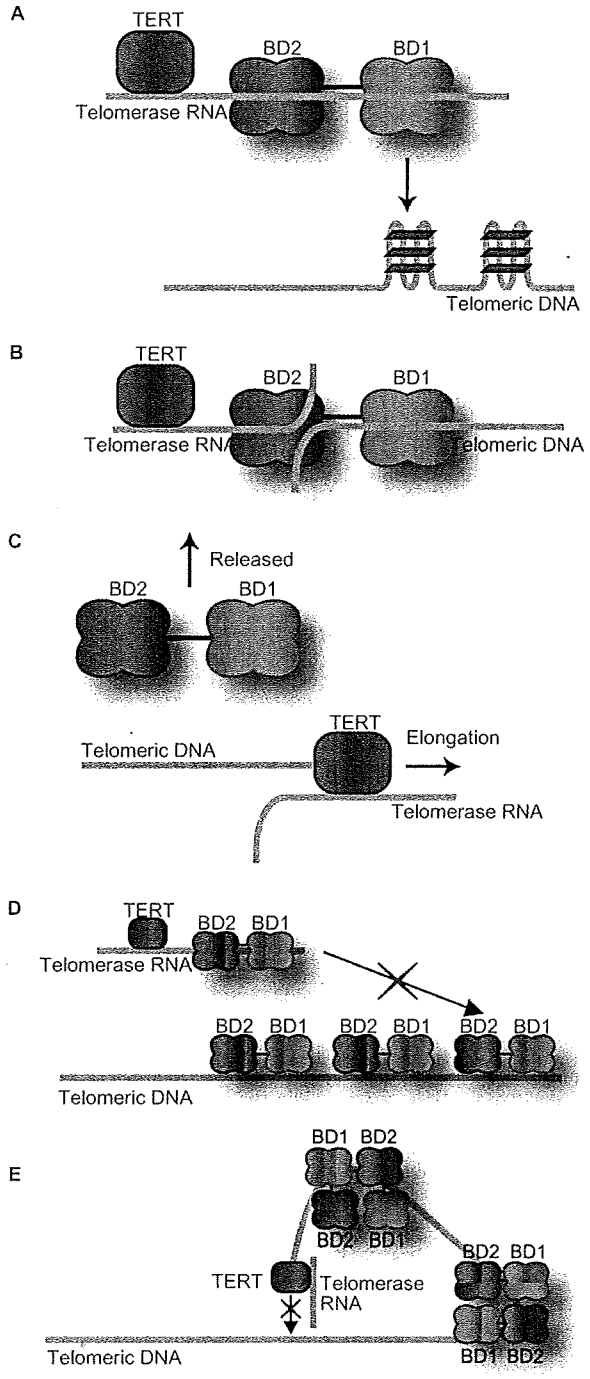

Figure 5. A model for how hnRNP A1/UP1 both enhances and represses the telomerase activity. A model for enhancement of the telomerase activity through the recruitment of telomerase to telomeric DNA by UP1 composed of BD1 and BD2 (A–C). (A) UP1 captures telomerase through binding of both BD1 and BD2 to telomerase RNA. Telomerase-bound UP1 searches for telomeric DNA with the affinity of BDs, particularly that of BD1, to telomeric DNA. (B) When telomerase-bound UP1 encounters telomeric DNA, the BDs of UP1, particularly BD1, unfold the quadruplex structure of telomeric DNA into a single-stranded form. Then, UP1 bridges telomerase and telomeric DNA through simultaneous BD1 telomeric DNA and BD2 telomerase RNA interactions. (C) Telomerase brought to telomeric DNA forms the telomerase RNA telomeric DNA complex through their complementarity and begins to elongate the telomeric DNA. UP1 is released meanwhile. (D) An excess amount of UP1 may occupy the 3′-overhang of telomeric DNA and thus interfere with access of telomerase-bound UP1 to this region, which may result in the reduction of the telomerase activity. (E) When newly synthesized telomeric DNA becomes long, a certain higher order structure such as a loop structure may be formed with the assistance of UP1. The formed structure may sterically have an inhibitory effect on further elongation of telomeric DNA by telomerase. This may account for the reduction of the synthesis of longer telomeric DNA in the presence of UP1.

Another thing is that the synthesis of relatively long-telomeric DNA was repressed by UP1 (Figure 1). When the elongated telomeric DNA becomes longer, several distant parts of the elongated DNA may form a certain structure such as a loop structure with the assistance of UP1 (Figure 5E). It was found in the crystal structure that two telomeric DNA strands are brought close to each other through the interactions with a UP1 dimer (40). This kind of interaction could result in the formation of the loop structure. The formed structure may sterically inhibit further proceeding of telomerase, resulting in a decrease in the synthesis. Reduction of the synthesis of long-telomeric DNA caused by UP1 may be rationalized in this way. Alternative interpretation may also be possible. Binding of UP1 to single-stranded telomeric DNA might enhance the dissociation of telomerase from the telomeric DNA, which would result in the production of shorter telomeric DNA.

It may be the case that the enhancement of the synthesis of relatively short DNA is sufficient for hnRNP A1/UP1 to contribute to maintenance of the telomere *in vivo*. Alternatively, a not yet identified cellular factor, which was depleted during the course of the preparation of the telomerase extract as hnRNP A1 and hnRNP D were, may facilitate further enhancement by hnRNP A1/UP1 *in vivo*. For example, a factor that promotes the dissociation of hnRNP A1/UP1 from the telomeric DNA might be present in cells to guarantee the enhancement of the synthesis of relatively long DNA.

We found for the first time that UP1 has the ability to unfold the quadruplex structure of telomeric DNA into a single-stranded structure (24). On the basis of this finding, we proposed that UP1 may serve to enhance the telomerase activity through unfolding of the quadruplex structure of telomeric DNA and resultant provision of the accessible overhang (24). We also proposed a similar effect for a related protein, hnRNP D (26). We assume that both unfolding and recruitment by hnRNP A1/UP1 contribute to the enhancement of the telomerase activity and the maintenance of the proper telomeric DNA length. Thus, hnRNP A1/UP1, together with hnRNP D, may be promising targets for controlling the activity of telomerase which is linked to several cancers.

It must be a next target to determine the structures of the UP1–telomerase RNA and UP1–telomeric DNA binary complexes and the ternary complex. The effort is in progress to improve the relatively poor solubility and stability of these complexes.

ACKNOWLEDGEMENTS

We would like to thank Prof. Maeda, Dr Ohnishi, Dr Kobayashi and Mr Ohgara for their help in the preparation and NMR analysis with Kujira of UP1.

FUNDING

Ministry of Education, Science, Sports and Culture of Japan (19036026 to M.K., 2057011 to T.N.); Japan Science and Technology (PRESTO to M.K.); Yokohama City University (K20008 to M.K., W20011 to T.N.). Funding for open access charge: Ministry of Education, Science, Sports and Culture of Japan and Yokohama City University.

Conflict of interest statement. None declared.

REFERENCES

1. Makarov,V.L., Hirose,Y. and Langmore,L.P. (1997) Long G tails at both ends of human chromosomes suggest a C strand degradation mechanism for telomere shortening. *Cell*, **88**, 657–666.
2. McElligott,R. and Wellinger,R.J. (1997) The terminal DNA structure of mammalian chromosomes. *EMBO J.*, **16**, 3705–3714.
3. Blackburn,E.H. (2000) Telomere states and cell fates. *Nature*, **408**, 53–56.
4. van Steensel,B., Smogorzewska,A. and de Lange,T. (1998) TRF2 protects human telomeres from end-to-end fusions. *Cell*, **92**, 401–413.
5. Hackett,J.A., Feldser,D.M. and Greider,C.W. (2001) Telomere dysfunction increases mutation rate and genomic instability. *Cell*, **106**, 275–286.
6. Smogorzewska,A. and de Lange,T. (2004) Regulation of telomerase by telomeric proteins. *Annu. Rev. Biochem.*, **73**, 177–208.
7. Baumann,P. and Cech,T.R. (2001) Pot1, the putative telomere end-binding protein in fission yeast and humans. *Science*, **292**, 1171–1175.
8. Colgin,L.M., Baran,K., Baumann,P., Cech,T.R. and Reddel,R. (2003) Human POT1 facilitates telomere elongation by telomerase. *Curr. Biol.*, **13**, 942–946.
9. Loayza,D. and de Lange,T. (2003) POT1 as a terminal transducer of TRF1 telomere length control. *Nature*, **423**, 1013–1018.
10. Griffith,J. D., Comeau,L., Rosenfield,S., Stansel,R. M., Bianchi,A., Moss,H. and de Lange,T. (1999) Mammalian telomeres end in a large duplex loop. *Cell*, **97**, 503–514.
11. Kim,N.W, Piatyszek,M.A., Prowse,K.R., Harley,C.B., West,M.D., Ho,P.L., Coviello,G.M., Wright,W.E., Weinrich,S.L. and Shay,J.W. (1994) Specific association of human telomerase activity with immortal cells and cancer. *Science*, **266**, 2011–2015.
12. Phan,A.T., Kuryavyi,V. and Patel,D.J. (2006) DNA architecture: from G to Z. *Curr. Opin. Struct. Biol.*, **16**, 288–298.
13. Zahler,A.M., Williamson,J.R., Cech,T.R. and Prescott,D.M. (1991) Inhibition of telomerase by G-quartet DNA structures. *Nature*, **350**, 718–720.
14. Zaug,A.J., Podell,E.R. and Cech,T.R. (2005) Human POT1 disrupts telomeric G-quadruplexes allowing telomerase extension in vitro. *Proc. Natl Acad. Sci. USA*, **102**, 10864–10869.
15. Oganesian,L., Moon,I.K., Bryan,T.M. and Jarstfer,M.B. (2006) Extension of G-quadruplex DNA by ciliate telomerase. *EMBO J.*, **25**, 1148–1159.
16. Mayeda,A. and Krainer,A.R. (1992) Regulation of alternative pre-mRNA splicing by hnRNP A1 and splicing factor SF2. *Cell*, **68**, 365–375.
17. Mayeda,A., Munroe,S.H., Caceres,J.F. and Krainer,A.R. (1994) Function of conserved domains of hnRNP A1 and other hnRNP A/B proteins. *EMBO J.*, **13**, 5483–5495.
18. Yang,X., Bani,M.R., Lu,S.J., Rowan,S., Ben-David,Y. and Chabot,B. (1994) The A1 and A1B proteins of heterogeneous nuclear ribonucleoparticles modulate 5′ splice site selection *in vivo*. *Proc. Natl Acad. Sci. USA*, **91**, 924–6928.
19. Blanchette,M. and Chabot,B. (1999) Modulation of exon skipping by high-affinity hnRNP A1-binding sites and by intron elements that repress splice site utilization. *EMBO J.*, **18**, 1939–1952.
20. Izaurralde,E., Jarmolowski,A., Beisel,C., Mattaj,I.W., Dreyfuss,G. and Fischer,U. (1997) A role for the M9 transport signal of hnRNP A1 in mRNA nuclear export. *J. Cell Biol.*, **137**, 27–35.
21. LaBranche,H., Dupuis,S., Ben-David,Y., Bani,M.R., Wellinger,R.J. and Chabot,B. (1998) Telomere elongation by hnRNP A1 and a derivative that interacts with telomeric repeats and telomerase. *Nat. Genet.*, **19**, 199–202.
22. Patry,C., Bouchard,L., Labrecque,P., Gendron,D., Lemieux,B., Toutant,J., Lapointe,E., Wellinger,R. and Chabot,B. (2003) Small interfering RNA-mediated reduction in heterogeneous nuclear ribonucleoparticle A1/A2 proteins induces apoptosis in human cancer cells but not in normal mortal cell lines. *Cancer Res.*, **63**, 7679–7688.
23. Zhang,Q.S., Manche,L., Xu,R.M. and Krainer,A.R. (2006) hnRNP A1 associates with telomere ends and stimulates telomerase activity. *RNA*, **12**, 1116–1128.
24. Fukuda,H., Katahira,M., Tsuchiya,N., Enokizono,Y., Sugimura,T., Nagao,M. and Nakagama,H. (2002) Unfolding of quadruplex structure in the G-rich strand of the minisatellite repeat by the binding protein UP1. *Proc. Natl Acad. Sci. USA*, **99**, 12685–12690.
25. Myers,J.C., Moore,S.A. and Shamoo,Y. (2003) Structure-based incorporation of 6-methyl-8-(2-deoxy-beta-ribofuranosyl)isoxanthopteridine into the human telomeric repeat DNA as a probe for UP1 binding and destabilization of G-tetrad structures. *J. Biol. Chem.*, **278**, 42300–42306.
26. Enokizono,Y., Konishi,Y., Nagata,K., Ouhashi,K., Uesugi,S., Ishikawa,F. and Katahira,M. (2005) Structure of hnRNP D complexed with single-stranded telomere DNA and unfolding of the quadruplex by heterogeneous nuclear ribonucleoprotein D. *J. Biol. Chem.*, **280**, 18862–18870.
27. Fiset,S. and Chabot,B. (2001) hnRNP A1 may interact simultaneously with telomeric DNA and the human telomerase RNA *in vitro*. *Nucleic Acids Res.*, **29**, 2268–2275.
28. Tatematsu,K., Nakayama,J., Danbara,M., Shionoya,S., Sato,H., Omine,M. and Ishikawa,F. (1996) A novel quantitative 'stretch PCR assay' that detects a dramatic increase in telomerase activity during the progression of myeloid leukemias. *Oncogene*, **13**, 2265–2274.
29. Delaglio,F., Grzesiek,S., Vuister,G.W., Zhu,G., Pfeifer,J. and Bax,A. (1995) NMRPipe: a multidimensional spectral processing system based on UNIX pipes. *J. Biomol. NMR*, **6**, 277–293.
30. Garrett,D.S., Powers,R., Gronenborn,A.M. and Clore,G.M. (1991) A common sense approach to peak picking in two-, three-, and four-dimensional spectra using automatic computer analysis of contour diagrams. *J. Magn. Reson.*, **95**, 214–220.
31. Goddard,T.D. and Kneller,D.G. (2006) *SPARKY 3*, University of California, San Francisco.
32. Kobayashi,N., Iwahara,J., Koshiba,S., Tomizawa,T., Tochio,N., Guntert,P., Kigawa,T. and Yokoyama,S. (2007) KUJIRA, a package of integrated modules for systematic and interactive analysis of NMR data directed to high-throughput NMR structure studies. *J. Biomol. NMR*, **39**, 31–52.
33. Dellaire,F., Dupuis,S., Fiset,S. and Chabot,B. (2000) Heterogenous nuclear ribonucleoprotein A1 and UP1 protect mammalian telomeric repeats and modulate telomere replication *in vitro*. *J. Biol. Chem.*, **275**, 14509–14516.
34. Nagata,T., Kurihara,Y., Matsuda,G., Saeki,J., Kohno,T., Yanagida,Y., Ishikawa,F., Uesugi,S. and Katahira,M. (1999) Structure and interactions with RNA of the N-terminal UUAG-specific RNA-binding domain of hnRNP D0. *J. Mol. Biol.*, **287**, 221–237.
35. Katahira,M., Miyanoiri,Y., Enokizono,Y., Matsuda,G., Nagata,T., Ishikawa,F. and Uesugi,S. (2001) Structure of the C-terminal RNA-binding domain of hnRNP D0 (AUF1), its interactions with RNA and DNA, and change in backbone dynamics upon complex formation with RNA. *J. Mol. Biol.*, **311**, 973–988.
36. Garrett,D.S., Lodi,P.J., Shamoo,Y., Williams,K.R., Clore,G.M. and Gronenborn,A.M. (1994) Determination of the secondary structure and folding topology of an RNA binding domain of mammalian hnRNP A1 protein using three-dimensional heteronuclear magnetic resonance. *Biochemistry*, **33**, 2852–2858.

37. Wishart,D.S., Sykes,B.D. and Richards,F.M. (1992) The chemical shift index: a fast and simple method for the assignment of protein secondary structure through NMR spectroscopy. *Biochemistry*, **18**, 1647–1651.
38. Shamoo,Y., Krueger,U., Rice,L.M., Williams,K.R. and Steitz,T.A. (1997) Crystal structure of the RNA binding domains of human hnRNP A1 at 1.75 Å resolution. *Nat. Struct. Biol.*, **4**, 215–222.
39. Xu,R.M., Jokhan,L., Cheng,X., Mayeda,A. and Krainer,A. (1997) Crystal structure of human UP1, the domain of hnRNP A1 that contains two RNA-recognition motifs. *Structure*, **5**, 559–570.
40. Ding,J., Hayashi,M.K., Zhang,Y., Manche,L., Krainer,A.R. and Xu,R.M. (1999) Crystal structure of the two-RRM domain of hnRNP A1 (UP1) complexed with single-stranded telomeric DNA. *Genes Dev.*, **13**, 1102–1115.
41. Moran-Jones,K., Wayman,L., Kennedy,D.D., Reddel,R.R., Sara,S., Snee,M.J. and Smith,R. (2005) hnRNP A2, a potential ssDNA/RNA molecular adapter at the telomere. *Nucleic Acids Res.*, **33**, 486–496.
42. Zaug,A.J., Podell,E.R. and Cech,T.R. (2005) Human POT1 disrupts telomeric G-quadruplexes allowing telomerase extension *in vivo*. *Proc. Natl Acad. Sci. USA*, **102**, 10864–10869.

β-catenin is strongly elevated in rat colonic epithelium following short-term intermittent treatment with 2-amino-1-methyl-6-phenylimidazo[4,5-*b*]pyridine (PhIP) and a high-fat diet

Rong Wang,[1] W. Mohaiza Dashwood,[1] Christiane V. Löhr,[2] Kay A. Fischer,[2] Hitoshi Nakagama,[3] David E. Williams[1,4] and Roderick H. Dashwood[1,4,5]

[1]Linus Pauling Institute, [2]College of Veterinary Medicine, Oregon State University, Corvallis OR 97331-6512; [3]Biochemistry Division, National Cancer Center Research Institute, 1-1, Tsukiji 5-chome, Chuo-ku, Tokyo 104-0045, Japan; [4]Department of Environmental and Molecular Toxicology, Oregon State University, Corvallis OR 97331-6512, USA

(Received April 2, 2008/Revised April 24, 2008; May 13, 2008/Accepted May 13, 2008/Online publication July 4, 2008)

Colon tumors expressing high levels of β-catenin and c-myc have been reported in male F344 rats given three short cycles of 2-amino-1-methyl-6-phenylimidazo[4,5-*b*]pyridine (PhIP) alternating with a high-fat (HF) diet. Using the same experimental protocol, rats were euthanized 24 h after the last dose of PhIP so as to examine early changes in colonic crypt homeostasis and β-catenin expression, before the onset of frank tumors. PhIP/HF dosing caused a significant increase in the bromodeoxyuridine labeling index throughout the entire colon, and within the colonic crypt column cleaved caspase-3 was elevated in the basal and central zones, but reduced in the luminal region. In vehicle/HF controls, β-catenin was immunolocalized primarily at the border between cells at the top of the crypt, whereas in rats given PhIP/HF diet there was strong cytoplasmic staining, which appeared as a gradient of increased β-catenin extending from the base of the crypt column to the luminal region. Quantitative real-time PCR and immunoblot analyses confirmed that β-catenin and c-myc were increased significantly in the colonic mucosa of rats given PhIP/HF diet. Collectively, these findings suggest that PhIP/HF cycling alters β-catenin and c-myc expression in the colonic mucosa, resulting in expansion of the proliferative zone and redistribution of apoptotic cells from the lumen to the central and basal regions of the colonic crypt. Thus, during the early stages of colon carcinogenesis, alternating exposure to heterocyclic amines and a high-fat diet might facilitate molecular changes resulting in dysregulated β-catenin and c-myc expression. (*Cancer Sci* 2008; 99: 1754–1759)

High-temperature cooking of meat and fish generates heterocyclic amine mutagens,[1] including the compound 2-amino-1-methyl-6-phenylimidazo[4,5-*b*]pyridine (PhIP).[2] PhIP is a multiorgan carcinogen in the rat, inducing tumors of the colon, prostate, mammary gland and other sites.[3] These tumors are characterized by high expression levels of β-catenin and β-catenin/T-cell factor (Tcf) target genes,[4–7] as seen in primary human colon cancers and human colorectal cancer cell lines.[8–10]

Recently, it was reported that three short cycles of PhIP alternating with a high-fat (HF) diet was as effective for the induction of colon tumors as continuous dietary treatment with the carcinogen.[11,12] It was speculated that with continuous PhIP administration, multiple disadvantageous mutations might interfere with the growth of focal populations, resulting in cell death, so that only a subset of transformed cells survive and proliferate. It was suggested that intervals between PhIP exposure might produce 'less chance of lethal mutations occurring [and] high-fat diet could directly promote cell growth'.[11] This selection process might be further influenced by postinitiation exposure to dietary phytochemicals, so that certain oncogenic mutants progress in preference to others, such as those affecting β-catenin stability.[7,12]

To provide insight into the possible selection pressures during early stages of colon carcinogenesis, we examined the effects of short-term intermittent PhIP/HF diet exposure on colonic cell homeostasis in the rat, before the onset of frank colon tumors. We report here on the induction of cell proliferation and apoptosis within the proliferative zone of the colonic crypt, with strongly elevated levels of cytoplasmic and nuclear β-catenin. There was a concomitant increase in β-catenin and c-myc mRNA and protein expression, consistent with results obtained in colon tumors at 1 year.[12]

Materials and Methods

Animals and treatment. Prior approval was obtained from the Institutional Animal Care and Use Committee. The treatment protocol is illustrated in Fig. 1, and full details were reported recently by Wang *et al.*[12] In brief, male F344 rats obtained at 4–5 weeks of age from the US National Cancer Institute were housed two per cage and given AIN93G diet (Dyets Inc., Bethlehem, PA) and water *ad libitum*. After 1 week acclimatization to the cages, PhIP (Toronto Research Chemicals, Ontario, Canada) was administered to each rat by daily oral gavage at a dose of 50 mg/kg body weight, which approximates the daily exposure in rats given 400 parts per million (p.p.m.) PhIP in the diet.[3] Controls received vehicle alone (0.8% dimethyl sulfoxide [DMSO] in ultra-pure water, adjusted to pH 3.5 with 0.1 N HCl). Following 2 weeks of PhIP or vehicle treatment, rats were placed on AIN93G diet supplemented with Primex hydrogenated vegetable oil, comprising 23% fat-derived calories, and referred to hereafter as high-fat (HF) diet. This diet was obtained from a commercial vendor (Dyets Inc., Bethlehem, PA, USA), and the composition is shown in Table 1. After 4 weeks on HF diet, animals were returned to standard AIN93G diet and treated again with PhIP or vehicle for 2 weeks, followed by an additional 4 weeks on HF diet. A third cycle of PhIP or vehicle then was completed, and 24 h later the rats were euthanized by CO_2 inhalation. Colons from four

[5]To whom correspondence should be addressed.
E-mail: Rod.Dashwood@oregonstate.edu

doi: 10.1111/j.1349-7006.2008.00887.x

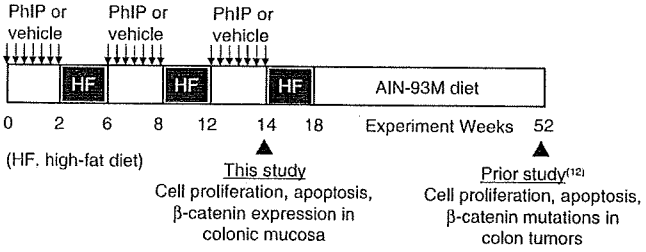

Fig. 1. Experimental protocol for short-term intermittent 2-amino-1-methyl-6-phenylimidazo[4,5-*b*]pyridine (PhIP) treatment alternating with high-fat diet. This figure was modified from a recent report by Wang *et al.*, which provided full details of the treatment protocol.[12] In brief, male F344 rats were given PhIP by daily oral gavage at a dose of 50 mg/kg body weight, whereas controls received vehicle alone (0.8% dimethyl sulfoxide [DMSO] in ultra-pure water, adjusted to pH 3.5 with 0.1 N HCl). Following 2 weeks of PhIP or vehicle treatment, rats were placed on AIN93G diet supplemented with Primex hydrogenated vegetable oil, comprising 23% fat-derived calories (high-fat [HF] diet). After 4 weeks on HF diet, animals were returned to standard AIN93G diet and treated again with PhIP or vehicle for 2 weeks, followed by an additional 4 weeks on HF diet. A third cycle of PhIP or vehicle then was completed, and 24 h later the rats were euthanized by CO_2 inhalation. Note: in our prior study, which lasted 1 year,[12] rats were switched as recommended from AIN93G (growth) diet to AIN94M (maintenance) diet at week 18.

PhIP-treated rats and three vehicle-treated rats were Swiss-rolled and fixed in 10% formalin for immunohistochemical analyses. Colons from five additional PhIP-treated rats and six vehicle-treated rats were opened longitudinally, and the mucosa was scraped and frozen in liquid nitrogen, then stored at –80°C for subsequent molecular work.

Scoring of cell proliferation and apoptosis indices. Details of the methods used for tissue isolation and immunohistochemistry were reported elsewhere.[12] In brief, 5–6 rats in each group were selected at random and injected *i.p.* with bromodeoxyuridine (BrdU, 200 μmol/kg body wt), 1 h before sacrifice. Colons were removed and processed for immunostaining using the BrdU *in situ* detection kit (BDBiosciences, San Jose, CA, USA). In addition, cleaved caspase-3 was immunolocalized using the EnVision+System-HRP Kit (Dako, Carpinteria, CA, USA) in conjunction with a polyclonal rabbit anticleaved caspase-3 antibody, which detects the endogenous large fragment of cleaved caspase-3 resulting from cleavage adjacent to Asp175 (Cell Signaling Inc., Danvers, MA, USA). Labeling indices were calculated as the number of positive cells divided by the total number of cells in the basal, central and apical regions of the colonic crypt column, for a minimum of 15 crypts in each of the distal, middle and proximal regions of the colon (=45 crypts scored per colon). Only complete, well-oriented, longitudinally sectioned crypts were evaluated.

Immunohistochemical detection of β-catenin. The basic method was identical to that used for cleaved caspase-3, but with polyclonal rabbit antiβ-catenin (Abcam, ab2982, Cambridge, MA, USA) at 500-fold dilution in phosphate-buffered saline.

Quantitative real-time PCR (qPCR). *Ctnnb1* (β-catenin), *cyclin D1*, c-*myc* and c-*jun* mRNA levels were determined by quantitative (q)PCR and normalized to glyceraldehyde-3-phosphate dehydrogenase (*Gapdh*), exactly as reported.[5,12] In brief, frozen samples of colonic mucosa (5–6 rats per group) were thawed and the mRNA was extracted using the RNeasy kit (Qiagen, Valencia, CA, USA). RNA was reverse-transcribed using Omniscript Reverse Transcriptase (Qiagen) and random hexamers (Invitrogen). PCR was conducted on an Opticon Monitor 2 system (Finnzymes, Finland), in 20 μL total reaction volume containing cDNAs, SYBR Green I dye (DyNAmo master solution, Finnzymes) and gene-specific primers. The amount of specific mRNA was quantified by determining the point at which the fluorescence accumulation entered the exponential phase (C_t), and the C_t ratio of the target gene to *Gapdh* was calculated for each sample. Three separate experiments were performed for each sample, and the corresponding results were expressed as mean ± SE.

Immunoblotting. β-Catenin, c-myc, c-jun and cyclin D1 were examined using the immunoblotting methodology reported elsewhere, with β-actin as loading control.[6,7]

Statistics. Data were plotted as mean ± SE and compared using Students *t*-test. In the figures, significant *P*-values are shown as follows: $*P < 0.05$, $**P < 0.01$, $***P < 0.001$.

Results

Cycling of PhIP/HF diet strongly induces cell proliferation throughout the colon. Immunohistochemical staining for BrdU incorporation revealed a marked difference between vehicle- and PhIP-treated rats (Fig. 2). When quantified for the entire crypt column (Fig. 2a), the BrdU labeling index showed a highly significant increase in rats given PhIP in the proximal, middle and distal regions of the colon. Specifically, 6–9% of the cells were BrdU-positive in vehicle controls, compared with 14–19% in rats given PhIP. BrdU-positive cells also were quantified for different regions within the crypt column (Fig. 2b–d); increased labeling was seen in the central and basal regions, with little or no change in the luminal zone (upper-third).

Cycling of PhIP/HF diet alters the distribution of apoptotic cells within the colonic crypt. Immunohistochemical staining for cleaved caspase-3, a marker of apoptosis, identified positive cells along the uppermost region of the crypt in vehicle controls, and more generalized staining throughout the crypt column in rats given PhIP (Fig. 3). Quantification of the labeling index for the entire crypt column showed no significant differences in the proximal, middle or distal regions of the colon (Fig. 3a). However, when

Table 1. Composition of AIN93G and high-fat (HF) AIN93G diets

Ingredient	AIN93G (Dyets #110700) g/kg	HF AIN93G (Dyets #181059) g/kg
Casein	200	200
L-Cystine	3	3
Sucrose	100	63.5
Cornstarch	397.486	252.186
Dyetrose	132	83.8
Soybean oil	70	70
t-Butylhydroquinone	0.014	0.014
Primex (hydrogenated vegetable.oil)	0	230
Cellulose	50	50
Mineral mix #210025	35	35
Vitamin mix #310025	10	10
Choline bitartrate	2.5	2.5
Total	1000	1000

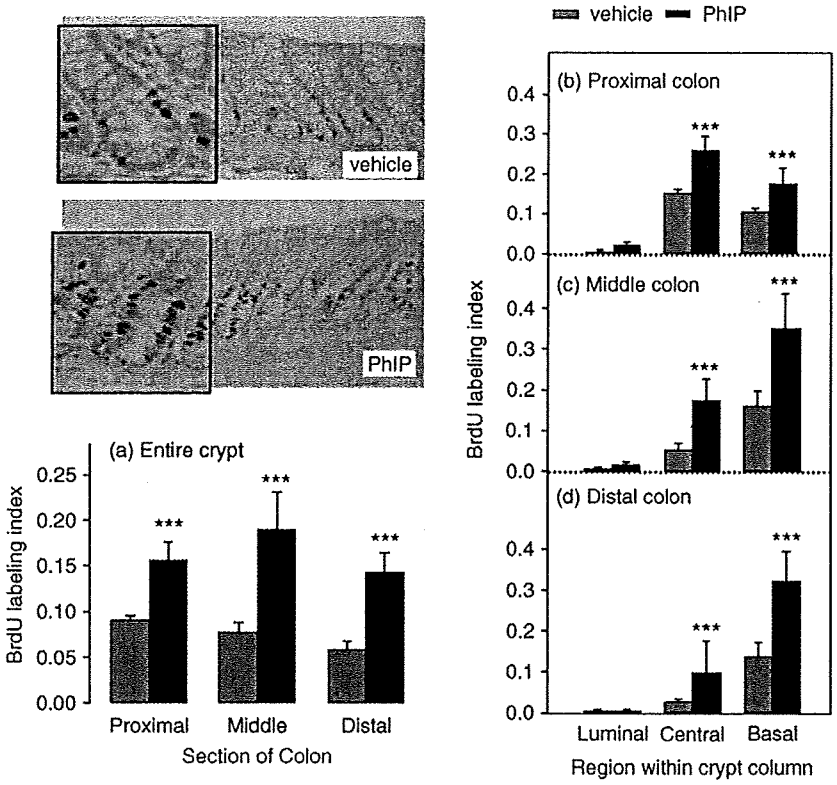

Fig. 2. Cycling of 2-amino-1-methyl-6-phenylimidazo[4,5-*b*]pyridine (PhIP)/high-fat diet induces cell proliferation in the colon. Rats were treated with PhIP and a high-fat diet (see Fig. 1) and the bromodeoxyuridine (BrdU) labeling index was determined as described in Materials and Methods. Data bars, mean ± SE; ***$P < 0.001$, by Students *t*-test, PhIP ($n = 4$) *versus* corresponding vehicle controls ($n = 3$).

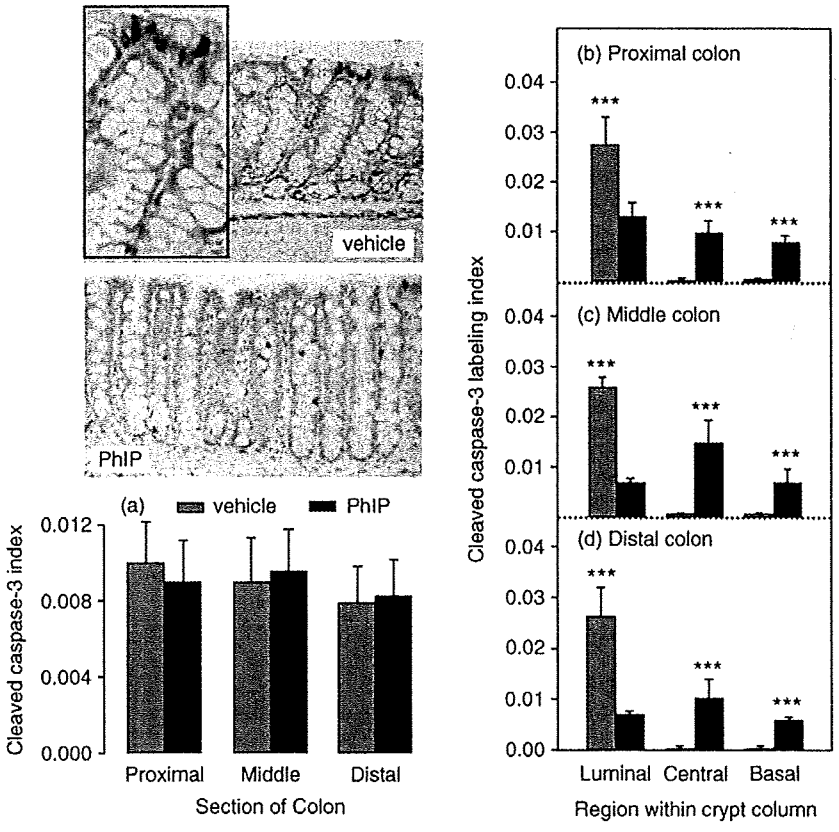

Fig. 3. Cycling of 2-amino-1-methyl-6-phenylimidazo[4,5-*b*]pyridine (PhIP)/high-fat diet increases cleaved caspase-3 labeling in the central and basal regions of the colonic crypt column and reduces it in the luminal region. The cleaved caspase-3 labeling index was determined as described in Materials and Methods. Data bars, mean ± SE; ***$P < 0.001$, by Students *t*-test, PhIP ($n = 4$) *versus* corresponding vehicle controls ($n = 3$).

doi: 10.1111/j.1349-7006.2008.00887.x

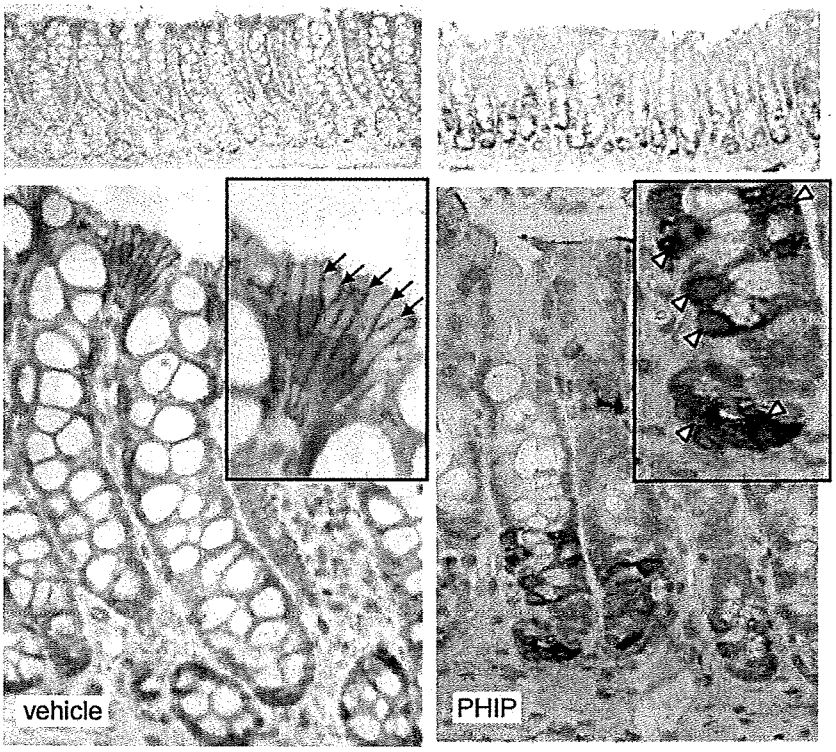

Fig. 4. Cycling of 2-amino-1-methyl-6-phenylimidazo[4,5-*b*]pyridine (PhIP)/high-fat diet increases β-catenin expression in the colon. Immunohistochemistry revealed low overall expression levels of β-catenin in vehicle controls, but high levels in PhIP-treated rats. In vehicle controls, β-catenin was restricted to the borders between cells (arrows), with little or no cytoplasmic and nuclear staining, whereas in PhIP-treated rats there was strong cytoplasmic β-catenin expression (arrow heads).

the cleaved caspase-3 labeling index was quantified for regions within the crypt column (Fig. 3b–d), a highly significant difference was seen between vehicle controls and PhIP-treated rats. In the latter case, cleaved caspase-3-positive cells were more-or-less evenly distributed throughout the luminal, central and basal crypt regions, whereas in vehicle controls the labeling was almost exclusively in the luminal region of the crypt. We interpret these data as evidence that PhIP/HF cycling increased cell proliferation in the lower two-thirds of the crypt (Fig. 2), giving rise to more apoptotic cells in the same region and a concomitant reduction in cell death at the top of the crypt.

Cycling of PhIP/HF diet increases β-catenin staining in the colonic crypt. An important regulator of cell proliferation and apoptosis in the colon is β-catenin and immunohistochemical staining revealed a marked difference in β-catenin expression within the crypt column of rats given PhIP compared with vehicle (Fig. 4). Thus, in vehicle controls, histological studies showed there was a generalized low level of β-catenin expression that was restricted to the borders between cells in the upper region of the crypt column (arrows), with no cytoplasmic or nuclear staining detected. In marked contrast, colons from rats given PhIP had widespread labeling throughout the lower half to two-thirds of the crypt column and β-catenin was strongly expressed in the cytoplasm and sometimes also in the nucleus (Fig. 4, open arrowheads).

Quantification of β-catenin-positive cells revealed significant differences between vehicle- and PhIP-treated rats. Specifically, in vehicle controls, <0.2% of the cells stained positive for nuclear and/or cytoplasmic β-catenin (grey bars, Fig. 5a), but ~78% of the cells were positive for membrane-associated β-catenin (grey bars, Fig. 5b), and this was seen in the proximal, middle and distal regions of the colon. In the proximal colon of PhIP-treated rats, 4% of the cells stained positive for nuclear/cytoplasmic β-catenin (solid bar, Fig. 5a) and ~25% for membrane-associated β-catenin (solid bar, Fig. 5b). In the middle colon, the corresponding data were 8–9% for nuclear/cytoplasmic β-catenin and 18.5% for membrane-associated β-catenin. In the distal colon of both PhIP- and vehicle-treated rats, ~75% of the cells stained positive for membrane-associated β-catenin (Fig. 5b), but few cells had nuclear/cytoplasmic staining.

Nuclear/cytoplasmic β-catenin labeling was further examined according to region within the colonic crypt column (Fig. 5c). There was evidence for a gradient of increased β-catenin expression in the colonic crypt of PhIP-treated rats compared with vehicle controls, with higher β-catenin levels in the basal zone than in the central or luminal zones. The data presented in Fig. 5(c) for PhIP-treated rats (solid bars) revealed 2%, 5.6% and 17.2% of the cells stained positive for nuclear/cytoplasmic β-catenin in the luminal, central and basal regions of the crypt, respectively ($P < 0.001$, each region *versus* the corresponding vehicle control).

Cycling of PhIP/HF diet elevates β-catenin and c-myc mRNA and protein expression. We next examined *Ctnnb1* (β-catenin) and three β-catenin/Tcf target genes, c-*myc*, c-*jun* and *cyclin D1*, for changes in mRNA expression (Fig. 6). Colonic mucosa from PhIP-treated rats had 30% higher levels of *Ctnnb1* and 65% higher levels of c-*myc* mRNA compared with vehicle controls ($P < 0.05$). No difference in c-*jun* or *cyclin D1* expression was observed after normalizing to *Gapdh*.

Immunoblotting revealed higher expression levels of β-catenin and c-myc proteins in colonic mucosa of PhIP-treated rats, compared with vehicle controls (Fig. 7). No differences were seen among the treatment groups for cyclin D1 and c-jun, after normalizing to β-actin (data not shown).

Discussion

Ubagai *et al.* studied the combined effects of PhIP and a HF diet on colon carcinogenesis in the F344 rat.[11] Animals were given 400 p.p.m. PhIP in the basal diet for 2 weeks, followed by HF diet for up to 110 weeks, and this resulted in 3 of 19 rats with large intestinal tumors (19% incidence). Alternatively, 400 p.p.m. dietary PhIP was given for 2 weeks, followed by 4 weeks on HF diet, and the PhIP/HF cycling was repeated three times, ending with continuous HF diet for up to 60 weeks. Large

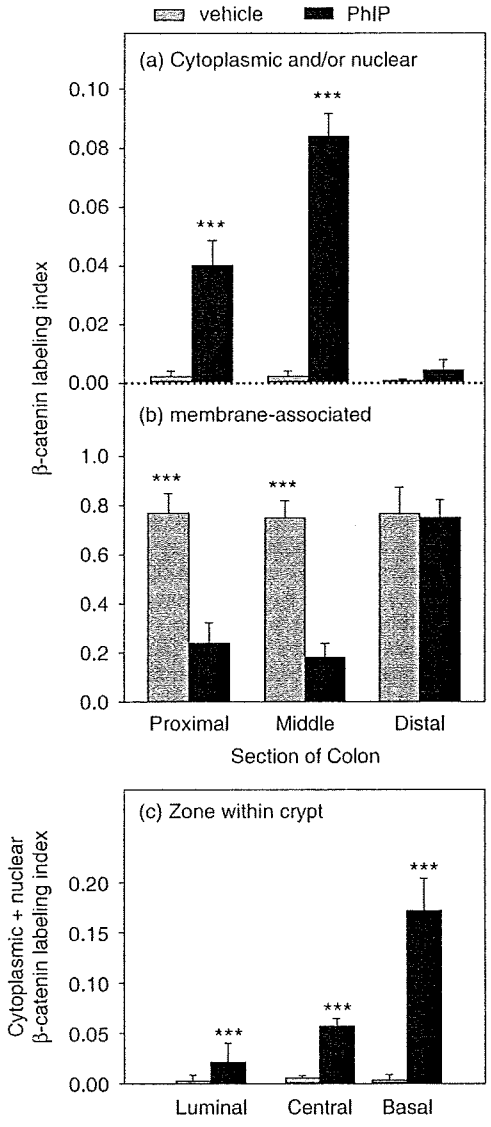

Fig. 5. Cycling of 2-amino-1-methyl-6-phenylimidazo[4,5-*b*]pyridine (PhIP)/high-fat diet increases cytoplasmic β-catenin expression in the colon. The β-catenin labeling index was scored as the number of cells stained positively for cytoplasmic (and/or nuclear) *versus* membrane-associated expression, divided by the total number of cells in that region of the colon. Data bars, mean ± SE; PhIP $n = 4$, vehicle controls $n = 3$. $^{**}P < 0.01$; $^{***}P < 0.001$, PhIP group significantly different from the corresponding vehicle controls.

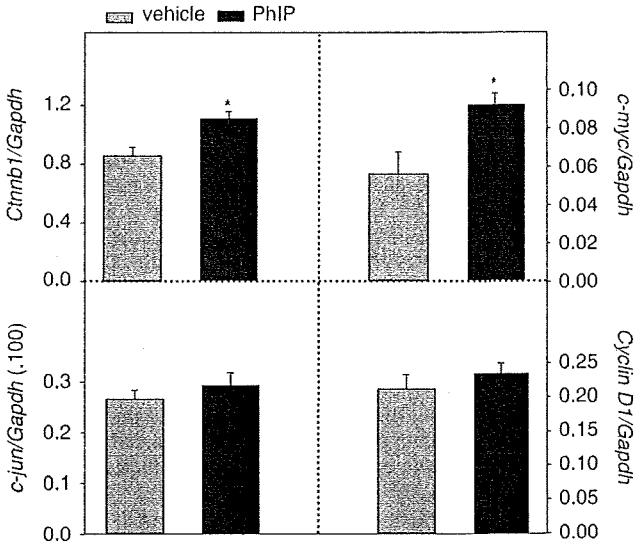

Fig. 6. Cycling of 2-amino-1-methyl-6-phenylimidazo[4,5-*b*]pyridine (PhIP)/HF diet increases β-catenin and c-myc mRNA expression in the rat colon. Quantitative real-time PCR was performed as described in Materials and Methods, for β-catenin (*Ctnnb1*) and three β-catenin/Tcf target genes, namely c-*myc*, c-*jun* and *cyclin D1*, normalized to *Gapdh*. Data bars, mean ± SE, PhIP $n = 5$, vehicle controls $n = 6$. $^{*}P < 0.05$, PhIP group significantly different from corresponding vehicle controls.

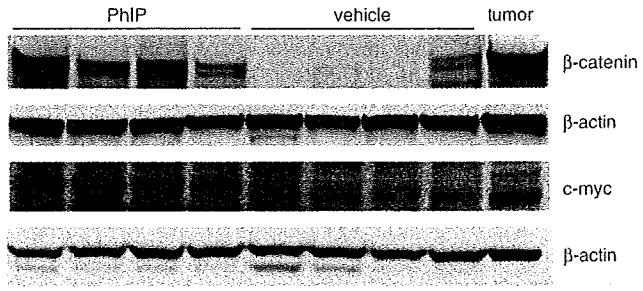

Fig. 7. Immunodetection of increased β-catenin and c-myc in the rat colon before the onset of frank tumors. Representative immunoblots of β-catenin and c-myc in colonic mucosa from rats treated with three cycles of 2-amino-1-methyl-6-phenylimidazo[4,5-*b*]pyridine (PhIP) (or vehicle) alternating with high-fat diet. A PhIP-induced colon tumor from the corresponding 1-year carcinogenicity study,[12] is shown in the furthest right lane as a positive control. β-Actin, loading control.

intestinal tumors were seen in 9 out of 20 rats (45% incidence). The latter result compares favorably with the 43% incidence observed in rats treated continuously with 100 p.p.m. dietary PhIP for 104 weeks,[3] in which a ~10-fold greater total amount of PhIP was administered per animal. Thus, PhIP/HF cycling represents an efficient means of inducing colon tumors, using a fraction of the amount of total carcinogen. We further modified the experimental protocol by giving PhIP via oral gavage, at a dose (50 mg/kg body wt per day) that was matched to the daily carcinogen intake from 400 p.p.m. PhIP in the diet,[3] and after three cycles of PhIP/HF treatment, standard AIN93M diet rather than HF diet was administered. Using this modified protocol, the colon tumor incidence after 1 year was 41.6%.[12]

In the current investigation, rats were euthanized immediately after completing the third and final cycle of PhIP dosing, so as to examine changes in colonic crypt homeostasis before the onset of frank tumors. Under these conditions, there was a striking increase in BrdU-positive cells throughout the entire length of the colon, with particularly high staining in the lower two-thirds of the crypt column. Moreover, there was an increase in cleaved caspase-3-positive cells in the proliferative zone of each crypt (central and basal regions), coupled with a reduction of apoptotic cells in the luminal region. The present study was not designed to specifically compare intermittent PhIP/HF dosing with continuous dietary PhIP treatment, but this might be interesting in a follow up investigation. Previously, a modest 1.5-fold increase in colonic BrdU labeling was seen at 8 weeks in male (but not female) rats fed continuously with 400 p.p.m. PhIP in the diet, and no significant changes were seen in cell proliferation rates for male or female rats at 4 or 12 weeks.[13] However, the latter

doi: 10.1111/j.1349-7006.2008.00887.x

study did not assess changes in apoptosis or β-catenin expression. In general, we observed that cleaved caspase-3 did not show as good a concordance as did BrdU labeling for the corresponding β-catenin positive cells.

The high cytoplasmic β-catenin expression seen in the present study is noteworthy, because Ubagai *et al.*[11] reported that all of the large intestinal tumors obtained following PhIP/HF treatment also had high accumulation of cytoplasmic and nuclear β-catenin. Interestingly, only 55% of the tumors harbored a mutation in the *Apc* or *Ctnnb1* (β-catenin) genes, and it was suggested that PhIP/HF cycling produced 'unknown genetic alterations' in the Wnt–Apc–β-catenin signaling pathway.[11] Using the identical exposure protocol described here, colon tumors obtained at 1 year had a 36% frequency of β-catenin mutations, although this was increased to 79% when rats were subjected to postinitiation treatment with caffeine, which resulted in tumor promotion.[12] This clearly supports the notion that cells harboring specific genetic changes within a population can be influenced to progress (or not to progress) to neoplasia by external factors, such as phytochemicals and a HF diet. As discussed before,[11] intermittent exposure to PhIP might allow populations of cells to survive and progress to tumors, when continuous carcinogen treatment might otherwise lead to removal of those cells via apoptosis. In the present study, there was increased apoptosis in the lower half of the colonic crypt following PhIP cycling, but this appeared to be a compensatory mechanism triggered by the greatly enhanced rate of cell proliferation, resulting in expansion of the crypt-wide proliferative zone (Fig. 2).

Despite the high levels of β-catenin detected in the present study following PhIP/HF treatment (Fig. 4), no β-catenin mutations were observed in the colonic mucosa scrapings, using PCR-based single strand conformation polymorphism (PCR-SSCP) screening (data not presented). One interpretation is that β-catenin mutations were indeed present in the colonic scrapings, but below the limit of detection of the PCR-SSCP methodology, and that only after clonal expansion and tumor formation were the mutations readily detected owing to their enrichment relative to the wild type allele. Interestingly, among the three reported β-catenin/Tcf target genes examined, only c-*myc* was increased in the colonic mucosa of rats given PhIP/HF diet, as noted in the colon tumors obtained at 1 year.[12] Interestingly, *Ctnnb1* mRNA also was elevated in the colonic mucosa of rats given PhIP/HF diet (Fig. 6). Although this increase was modest, it is consistent with prior reports showing elevated levels of *Ctnnb1* mRNA expression in PhIP- and 1,2-dimethylhydrazine-induced rat colon tumors,[5,12] as well as in primary human colon carcinomas and their liver metastases.[14] In some of the vehicle controls, low or undetectable levels of β-catenin were seen via immunoblotting (Fig. 7), despite the presence of *Ctnnb1* mRNA in most samples (Fig. 6) and membrane-associated β-catenin being detected in immunohistochemical analyses (Fig. 4). It is unclear whether this reflects the efficiency of the membrane extraction and/or immunoblot procedures used here, and further work is needed to clarify this question, perhaps on a larger subset of tissue samples from vehicle and PhIP-treated animals. However, for the vehicle control samples shown here (Fig. 7), repeated immunoblotting confirmed the low or undetectable expression of β-catenin, suggesting the data in this case were reproducible.

In summary, we have shown that in rats given three cycles of PhIP alternating with exposure to HF diet, there was an increase in colonic cell proliferation, elevated apoptosis in the proliferative zone of the colonic crypt and augmented expression of cytoplasmic β-catenin. These results from the early stages of colon carcinogenesis suggested a possible independent dysregulation of β-catenin and c-myc expression, separate from the classical β-catenin/Tcf pathway,[15] in accordance with data obtained from the corresponding colon tumors at 1 year.[12] Thus, early changes affecting colonic crypt homeostasis at the time of exposure to PhIP and HF diet may have persisted into much later stages of colon tumor formation.

Acknowledgments

We thank Mandy Louderback for assistance with oral gavage and necropsy. Laboratory Animal Service (LAR) staff are gratefully acknowledged for their help with animal care and maintenance. The experiments described here were supported in part by NIH grants CA90890, CA65525, CA90176 and CA122959, and by National Institute of Environmental Health Sciences Center grant P30 ES00210. Partial support for RHD was provided by the Foundation for Promotion of Cancer Research, Tokyo, Japan.

References

1 Sugimura T, Wakabayashi K, Nakagama H, Nagao M. Heterocyclic amines: mutagens/carcinogens produced during cooking of meat and fish. *Cancer Sci* 2004; **95**: 290–9.
2 Knize MG, Felton JS. Formation and human risk of carcinogenic heterocyclic amines formed from natural precursors in meat. *Nutr Rev* 2005; **63**: 158–65.
3 Ito N, Hasegawa R, Imaida K *et al.* Carcinogenicity of 2-amino-1-methyl-6-phenylimidazo[4,5-*b*]pyridine (PhIP) in the rat. *Mutat Res* 1997; **376**: 107–14.
4 Dashwood RH, Suzui M, Nakagama H, Sugimura T, Nagao M. High frequency of β-catenin (*Ctnnb1*) mutations in the colon tumors induced by two heterocyclic amines in the F344 rat. *Cancer Res* 1998; **58**: 1127–9.
5 Wang R, Dashwood WM, Bailey GS, Williams DE, Dashwood RH. Tumors from rats given 1,2-dimethylhydrazine plus chlorophyllin or indole-3-carbinol contain transcriptional changes in β-catenin that are independent of β-catenin mutation status. *Mutat Res* 2006; **601**: 11–18.
6 Blum CA, Tanaka T, Zhong X *et al.* Mutational analysis of *Ctnnb1* and *Apc* in tumors from rats given 1,2-dimethylhydrazine or 2-amino-3-methylimidazo[4,5-*f*]quinoline: mutational 'hotspots' and the relative expression of β-catenin and c-jun. *Mol Carcinogen* 2003; **36**: 195–203.
7 Blum CA, Xu M, Orner GA *et al.* β-Catenin mutation in rat colon tumors initiated with 1,2-dimethylhydrazine and 2-amino-3-methylimidazo[4,5-*f*]quinoline, and the effect of post-initiation treatment with chlorophyllin and indole-3-carbinol. *Carcinogenesis* 2001; **22**: 315–20.
8 Segditsas S, Tomlinson I. Colorectal cancer and genetic alterations in the Wnt pathway. *Oncogene* 2006; **25**: 7531–7.
9 Gavert N, Ben-Ze'ev A. beta-Catenin signaling in biological control and cancer. *J Cell Biochem* 2007; **102**: 820–8.
10 Wood LD, Parsons DW, Jones S *et al.* The genomic landscapes of human breast and colorectal cancers. *Science* 2007; **318**: 1108–13.
11 Ubagai T, Ochiai M, Kawamori T *et al.* Efficient induction of rat large intestinal tumors with a new spectrum of mutations by intermittent administration of 2-amino-1-methyl-6-phenylimidazo[4,5-*b*]pyridine in combination with a high-fat diet. *Carcinogenesis* 2002; **23**: 197–200.
12 Wang R, Dashwood WM, Löhr CV *et al.* Protective versus promotional effects of white tea and caffeine on PhIP-induced tumorigenesis and β-catenin expression in the rat. *Carcinogenesis* 2008; **29**: 834–9.
13 Ochiai M, Watanabe M, Kushida H, Wakabayashi K, Sugimura T, Nagao M. DNA adduct formation, cell proliferation, and aberrant crypt focus formation induced by PhIP in male and female rat colon with relevance to carcinogenesis. *Carcinogenesis* 1996; **17**: 95–8.
14 Mann B, Gelos M, Siedow A *et al.* Target genes of β-catenin-T cell-factor/lymphoid-enhancer-factor signaling in human colorectal carcinomas. *Proc Natl Acad Sci USA* 1999; **96**: 1603–8.
15 Yekkala K, Baudino TA. Inhibition of intestinal polyposis with reduced angiogenesis in ApcMin/+ mice due to decreases in c-Myc expression. *Mol Cancer Res* 2007; **5**: 1296–303.

Induction of multinucleated cells and apoptosis in the PC-3 prostate cancer cell line by low concentrations of polyethylene glycol 1000

Katsuhiro Fukuta,[1,2] Kenjiro Kohri,[2] Hirokazu Fukuda,[1] Masatoshi Watanabe,[3] Takashi Sugimura[1] and Hitoshi Nakagama[1,4]

[1]Biochemistry Division, National Cancer Center Research Institute, 5-1-1, Tsukiji, Chuo-ku, Tokyo 104-0045; [2]Department of Nephro-Urology, Nagoya City University Graduate School of Medical Sciences, 1, Kawasumi, Mizuho-cho, Mizuho-ku, Nagoya 467-8601; [3]Laboratory for Medical Engineering, Division of Materials Science and Chemical Engineering, Graduate School of Engineering, Yokohama National University, 79-1 Tokiwadai, Hodogaya-ku, Yokohama 240-8501, Japan

(Received December 27, 2007/Revised January 16, 2008/Accepted January 17, 2008/Online publication March 28, 2008)

Polyethylene glycol (PEG) has been reported to inhibit the development of colonic lesions in carcinogen-treated rats when administered orally. However, the precise mechanism for the chemopreventive activity of PEG remains largely elusive. Based on a characteristic feature of PEG as a 'fusogen', we investigated its potential as a chemotherapeutic agent through the induction of multinucleated cell formation and apoptosis induction in PC-3 prostate cancer cells. When PC-3 cells were treated with 0.5 and 1.0% PEG 1000, multinucleated cells were induced at a frequency of 8.4 and 13%, respectively, 36 h after PEG treatment under high cell density (1×10^6 cells in 100 μL PEG solution) *in vitro*. Although abnormality of cell cycle progression was not evident in PEG-treated PC-3 cells, multinucleated cells substantially disappeared at around 38 h due to apoptosis. In contrast, no apparent growth suppression was observed when PC-3 cells were exposed to up to 1.0% PEG at a much lower cell density, namely under ordinary culture conditions. Furthermore, injection of 0.5% PEG solution *in vivo* into PC-3 xenografts implanted in BALB/c-nu/nu male mice significantly suppressed tumor growth compared to phosphate-buffered saline injection. Multinucleated TdT-mediated dUTP-biotin nick end-labeling (TUNEL)-positive cells were observed inside the PEG-injected tumors. PEG was here demonstrated to have anticell proliferation and antitumor effects via induction of apoptosis, possibly by cell fusion. PEG injection therapy could therefore be adopted as an alternative chemotherapeutic strategy for localized prostate cancers, including those that become refractory to androgen-deprivation therapy. (*Cancer Sci* 2008; 99: 1055–1062)

Polyethylene glycol (PEG) has the chemical structure $H\text{-}(O\text{-}CH_2\text{-}CH_2)_n\text{-}OH$, and is known to be a nonabsorbed, non-toxic, and non-fermentable polymer.[1,2] Because PEG is non-toxic, it is used widely as a base material in, for example, skin creams and laxatives.[3,4] When PEG is bound to a hydrophobic molecule, a non-ionic detergent surfactant is obtained and can be used as an emulsion agent in cosmetics.[5] PEG is also used to encapsulate and solubilize hydrophobic compounds. It has recently been utilized in drug delivery systems, and PEGylation of interferon α (peginterferon α) and granulocyte colony-stimulating factor (pegfilgrastim) are now used for clinical applications.[6,7] The stability and hydrosolubility of various drugs is thereby markedly improved even under *in vivo* conditions. In the research field of biotechnology, PEG is also used for cell fusion as a 'fusogen'.[8,9]

In addition to these features, chemopreventive effects of PEG have been reported in rodent models of colon cancer.[10,11] When rats were treated with PEG 8000 after the administration of azoxymethane, a widely utilized colon carcinogen, a substantial decrease was observed in the number of aberrant crypt foci, putative precancerous lesions of the colon, and colon tumors.[12] Although the mechanistic interpretation for the chemopreventive effect of PEG is still controversial, several possibilities have been proposed. First, an increase in the gut content because of the high osmotic pressure in the digestive tract caused by the non-absorbed high molecular weight PEG could be a possibility, similar to dietary fiber.[10,13,14] Another possibility is that PEG may act directly on colon epithelial cells and exert some biological effects, such as induction of apoptosis, through osmotic pressure.[15]

In the present study, we examined whether PEG induces apoptosis in cancer cells using an androgen-independent human prostate cancer cell line, PC-3,[16] and could be used as an alternative therapeutic agent for human prostate cancers. Prostate cancer is a common cancer in men all over the world, and its incidence in Japan is currently increasing.[17,18] As for prostate cancer therapies, androgen-deprivation therapy (hormone therapy) now prevails all over the world, as it is non-invasive and relatively effective in many cases.[19–21] Radiation therapy, such as 'brachytherapy', is also used for localized prostate cancer.[22] However, these therapies have some drawbacks. For example, brachytherapy requires specific and well-guarded facilities for radiation. Hormone therapy is still quite costly, and androgen-independent prostate cancers arise frequently after continuous application of hormone therapy for a long period of time.[23] Establishment of safe and affordable therapies is therefore awaited.

Polyethylene glycol (PEG) has long been utilized to fuse different types of cells, as described above. Various cancer cells have been demonstrated to become fused by high concentrations (30–50%) of PEG.[24] We investigated whether the induction of apoptosis in cancer cells could result from such multinucleated cell formation as multinucleated cells induced by various cell-damaging agents, such as irradiation, doxorubicin, and docetaxel, have been shown to cause cell death by apoptosis.[25–27] We treated PC-3 cells under various conditions *in vitro* with PEG 1000 (refered to hereafter as 'PEG'). Interestingly, a concentration of PEG as low as 0.5–1.0% efficiently induced multinucleated cells under conditions of high cell density, and induced apoptosis after 34–38 h *in vitro*. PEG treatment at a low cell density ('ordinary culture conditions') was not similarly effective. When 0.5% PEG in phosphate-buffered saline (PBS) was injected directly into PC-3 xenografts in nude mice, tumor

[4]To whom correspondence should be addressed.
E-mail: hnakagam@gan2.res.ncc.go.jp

doi: 10.1111/j.1349-7006.2008.00781.x

growth was suppressed substantially compared to the PBS-injected control group. The potential molecular mechanisms underlying the suppressive effects of PEG on cell proliferation both *in vitro* and *in vivo* are discussed.

Materials and Methods

Chemicals. PEG and dimethylsulfoxide were obtained from Merck (Darmstadt, Germany), propidium iodide (PI), and etoposide were from Sigma (St Louis, MO, USA) and RNase A was from Qiagen (Valencia, CA, USA). DNA ladders of 100 bp (New England Biolabs, Beverly, MA, USA) and 1 kb (Promega, Madison, WI, USA) were used as molecular weight markers.

Cell culture. PC-3 cells were purchased from the American Type Culture Collection (ATCC; Manassas, VA, USA) and cultured at 37°C in Dulbecco's modified Eagle's medium (DMEM; Invitrogen Life Technologies, Carlsbad, CA, USA) supplemented with 10% heat-inactivated fetal bovine serum (FBS; Invitrogen Life Technologies), penicillin (100 U/mL), and streptomycin (50 U/mL) (Invitrogen Life Technologies) under a humidified atmosphere with 5% CO_2. DMEM (without FBS) was also used to make serial dilutions of PEG before addition into cell culture media.

Polyethylene glycol treatment protocol. PC-3 cells (1×10^6) were suspended in 100 μL of 0.5 and 1.0% PEG in DMEM (without FBS), incubated at room temperature for 1, 5, 15, or 30 min, then diluted 1:10 with DMEM and incubated at room temperature for 10 min. The cells were collected by centrifugation, gently washed twice with PBS, suspended in 10 mL of culture medium with FBS, seeded into 100-mm culture dishes with cover glasses at the bottom, and propagated for 34, 36, and 38 h. Cover glasses were then removed, the adherent cells on the cover glasses were fixed with 100% ethanol for 15 min, stained with PI solution (50 μg PI and 100 μg RNase A in 1.0 mL PBS), and then counted using a microscope. We adopted the criterion that cells having two or more nuclei were multinucleated. More than 500 cells within a randomly selected area on cover glasses were counted, and the cell counting was repeated three times for each experimental group.

Cell-growth assay. The effect of PEG on PC-3 cell growth was then evaluated under two different conditions. In the first condition, PC-3 cells (5×10^3) were plated in 100-mm culture dishes and incubated overnight ('ordinary culture conditions'). Aliquots of PEG in DMEM (1.0 mL) were added directly to cell culture dishes to give a final concentration of 0.5 or 1.0%, and the cells were propagated on the plates. As a reference control, 1.0 mL DMEM alone was added to the culture plates. The cells were harvested at 24, 36, 48, and 72 h after the addition of PEG, stained with trypan blue, and viable cell numbers were counted at each time point. Alternatively, 5×10^3 cells were treated following the PEG treatment protocol with 0, 0.5, or 1.0% PEG, seeded and propagated as above. In this case, cells were exposed to PEG for 1, 5, 15, and 30 min. Cells were then seeded in culture plates, propagated and harvested at 24, 36, 48, and 72 h after PEG treatment, including the nonadherent cells.

Detection of nuclear condensation. PC-3 cells were treated with 1.0% PEG for 30 min following the PEG treatment protocol, and seeded in 100-mm plates. Cells were collected after 34 h, fixed with 1.0% glutaraldehyde in PBS, incubated at 4°C overnight, collected by centrifugation, and resuspended in 50 μL PBS. After mixing thoroughly, 2 μL Hoechst 33258 (Dojindo, Kumamoto, Japan) was added to visualize nuclear condensation.

Poly(ADP-ribose) polymerase-1 cleavage. PC-3 cells were exposed to 0, 0.5, 1.0, or 2.0 PEG for 30 min, as described above. Cells were collected after 34 h and suspended in lysis buffer (50 mM Tris-HCl [pH 7.4], 150 mM NaCl, 1.0% Triton X-100) containing a protease inhibitor cocktail (Complete Mini; Roche, Indianapolis, IN, USA). Whole-cell lysates were electrophoresed on 5–20% linear gradient Tris-HCl-ready gels (Bio-Rad, Hercules, CA, USA) and fractionated proteins were transferred to polyvinylidene fluoride membranes (Immobilon-P; Millipore, Billerica, MA, USA). Western blot analysis was then carried out, as described elsewhere,[28] with mouse monoclonal antibody (mAb) against poly(ADP-ribose) polymerase (PARP)-1 (C2-10, 1:1000; Oncogene Research Products, San Diego, CA, USA) and mouse mAb against glyceraldehyde 3-phosphatase dehydrogenase (1:5000; Chemicon International, Temecula, CA, USA) as primary antibodies. For the secondary antibodies, horseradish peroxidase-conjugated antibodies against mouse IgG (NA9310V, 1:5000; Amersham Biosciences, Piscataway, NJ, USA) were used. Immunoreactive bands on the blots were visualized with chemiluminescence substrates (Immobilon Western; Millipore, Billerica, MA, USA). As a positive control, lysates were used from cells treated with a topoisomerase II inhibitor etoposide, which is known to induce apoptosis. Etoposide was dissolved in dimethylsulfoxide (25 mg/mL) and added to culture media to give a final concentration of 25 μg/mL.[29,30] Quantification of the cleaved PARP-1 protein was carried out using MultiGauge software (Fujifilm, Tokyo, Japan). Western blot analysis was carried out at least in triplicate.

Detection of DNA fragmentation. Following the PEG treatment protocol, PC-3 cells were exposed to 0, 0.5, 1.0, or 2.0% PEG for 30 min, seeded in 100-mm culture plates, and propagated for up to 38 h. Cells were collected, and DNA was extracted using a DNeasy Blood & Tissue Kit (Qiagen) following the manufacturer's instructions. Aliquots of extracted DNA samples were fractionated on a 1.5% SeaKem GTG agarose gel (Cambrex, Bio Science Rockland, Rockland, ME, USA). A DNA sample extracted from PC-3 cells treated with etoposide (25 μg/mL) for 48 h was used as a positive control.

Quantification of apoptosis by flow cytometry. PC-3 cells were treated with 0.5 or 1.0% PEG for 1 min following the PEG treatment protocol, seeded in 100-mm culture dishes and propagated in DMEM media without PEG for 36 h. Cells were harvested, washed gently with PBS, collected by centrifugation, and then stained using a MEBCYTO Apoptosis Kit (MBL, Nagoya, Japan) following the manufacturer's instructions. Cells were doubly stained with Annexin-V and PI, and the fluorescence intensities were measured by flow cytometry (FCM) (FACScan; BD Bioscience, San Jose, CA, USA) using the CellQuest analysis program.[31] We also conducted FCM analyses as above to evaluate the populations of apoptotic cells specifically among the large cells. Briefly, fluorescence intensities of the PI signal in DMEM-treated PC-3 cells were extracted from FCM data sets, expressed using FL-2A (representing DNA content) and FL-2W (representing cell size), and gated by the R1 region (representing the large-cell population), the cut-off value for which was set arbitrarily. The same scale was applied to the 0.5% PEG-treated cells. Cells extracted by the R1 region were replotted by PI signals against Annexin-V.

Cell cycle analyses by FCM. Following the PEG treatment protocol, PC-3 cells were exposed to 0, 0.5, 1.0, 2.0, or 10% PEG for 1 min, seeded in 100-mm culture plates, and propagated for 24, 34, 36, and 38 h. Cells were collected, fixed with 100% cold ethanol, and kept at –20°C overnight. After centrifugation, cells were resuspended in PI solution, incubated at room temperature for 15 min, and passed through nylon mesh (Becton, Dickinson and Company, Franklin Lakes, NJ, USA). The fluorescence intensities of PI were measured by FCM using a total of 20 000 PC-3 cells, and the number of cells in the sub-G_1, G_1, S, G_2/M, and >G_2/M (the population of cells with DNA contents beyond the G_2/M peak) fractions was counted at 24–38 h after PEG treatment. We further examined the number of PC-3 cells in large-cell populations and aneuploid populations using the same FCM data sets above at 34 and 36 h after PEG treatment.

doi: 10.1111/j.1349-7006.2008.00781.x

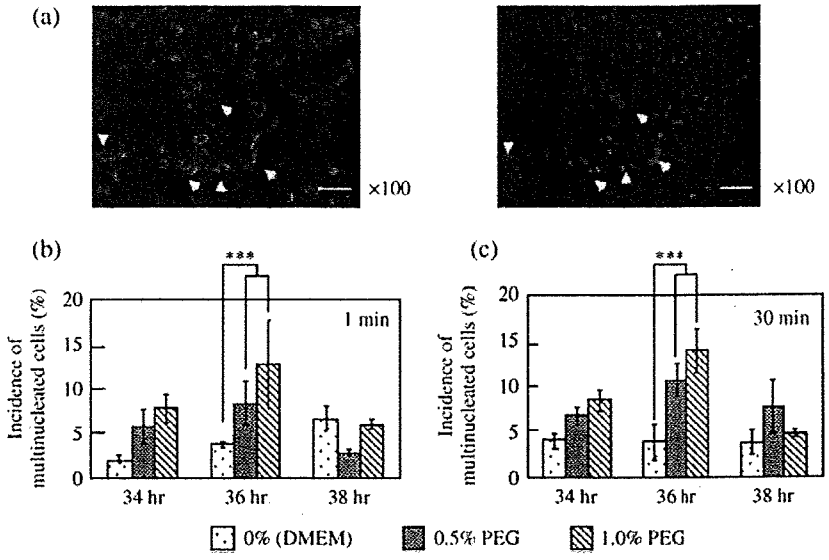

Fig. 1. Polyethylene glycol (PEG) induces multinucleated cells. (a) Following the PEG treatment protocol, PC-3 cells were treated with 0.5% PEG for 30 min. Cells were stained with propidium iodide (PI) (red). The left panel indicates the morphological features of the PEG-treated cells under microscopic observation with a green filter. The right panel indicates the nuclear staining of cells with PI. Both panels are the same magnification. The arrows indicate typical multinucleated cells. Scale bars = 50 μm. (b,c) Incidences of multinucleated cells in a total of 500 cells treated with PEG for (b) 1 min and (c) 30 min are shown. Values are the mean of fold ± SD. ***Differences of cell number between PEG treatment (0.5 and 1.0%) and the Dulbecco's modified Eagle's medium (DMEM)-treated control ($P < 0.001$).

Effects of PEG on in vivo tumor growth. The effect of PEG on PC-3 xenograft tumor growth was evaluated under two different conditions *in vivo*. With one of these, following the PEG treatment protocol, PC-3 cells (5×10^6 cells) were pretreated with DMEM or 0.5% PEG for 30 min, and then treated cells were implanted subcutaneously into the backs of BALB/c-nu/nu male mice (CLEA, Tokyo, Japan). Alternatively, PC-3 cells (5×10^6) were first implanted subcutaneously into the back of each mouse, and then at day 7 after implantation, 200-μL aliquots of PBS alone or 0.5% PEG solution in PBS were injected directly into the tumors using a 25-gauge injection needle (Terumo Corporation, Tokyo, Japan). Thereafter, tumors were measured twice a week throughout the experimental period of 19 days, and tumor volume was calculated using the following formula: (length [mm]) × (width [mm])^2 × 0.52. In these experiments, a total of 16 nude mice was randomly separated into four groups (4 × 4) receiving: DMEM treatment; 0.5% PEG treatment; intratumor PBS injection; and intratumor 0.5% PEG injection. PC-3 cells were implanted at two sites for each mouse. Animal experimental protocols were approved by the Committee for Ethics in Animal Experimentation, and the experiments were conducted in accordance with the guidelines for Animal Experiments of the National Cancer Center (Tokyo, Japan).

Histopathological analysis and detection of apoptosis in PC-3 xenografts. PC-3 xenografts were extirpated at 36–38 h after the last injection of PBS or 0.5% PEG for fixation in 10% neutralized formalin and embedding in paraffin blocks. Serial sections were prepared at 3.5-μm thickness, stained with hematoxylin and eosin (H&E), and subjected to histopathological analysis by a trained pathologist (M. W.). Apoptotic cells were detected using the TdT-mediated dUTP-biotin nick end-labeling (TUNEL) method,[32] which was carried out *in situ* using the DeadEnd Colorimetric TUNEL System (Promega) following the manufacturer's protocol.

Statistical analysis. All statistical analyses were carried out with Wilcoxon signed-ranks test using KaleidaGraph software (Synergy Software, Reading, PA, USA). Differences were considered significant when the *P*-value was less than 0.05.

Results

Induction of multinucleated PC-3 cells by PEG treatment *in vitro*. With the PEG treatment protocol, higher numbers of multinucleated cells were observed after PEG treatment, using 0.5–1.0% PEG (Fig. 1a). The incidence of multinucleated cells peaked at 36 h, being 8.4 and 13% with 0.5 and 1.0% PEG, respectively (Fig. 1b). The incidence only slightly increased with a longer exposure to PEG for 30 min (Fig. 1c).

Effects of PEG on PC-3 cell growth *in vitro*. In order to exclude possible toxic effects of PEG on PC-3 cells, we cultured PC-3 cells under two different culture conditions. When PC-3 cells were propagated under ordinary culture plates, and PEG was added into the media, no significant effect on cell growth was observed up to 72 h in the presence of 0.5 and 1.0% PEG, compared with the non-PEG treated control (Fig. 2a). However, significant differences were observed in cell growth between PEG-treated and DMEM-treated control cells when PC-3 cells were treated with 0.5% PEG (Fig. 2b) and 1.0% PEG (Fig. 2c) at a high cell density for 5–30 min, as in the PEG treatment protocol. A decrease in cell numbers became most prominent at around 36 h after PEG treatment (Fig. 2b,c).

Biochemical analyses for apoptosis. We observed nuclear condensation in multinucleated PC-3 cells on staining with Hoechst 33258 (Fig. 3a), suggesting induction of apoptosis.[33] Although DNA ladder formation was not observed in PEG-treated PC-3 cells, DNA samples extracted from the cells treated with PEG were substantially degraded compared to the DMEM-treated control (data not shown). Furthermore, PARP-1 cleavage, another characteristic feature of apoptosis,[34] was demonstrated in a PEG dose-dependent manner (Fig. 3b). The ratio of cleaved PARP-1 was increased by 14–52% in PEG-treated PC-3 cells when compared to the DMEM-treated control cells, although the increase was not so drastic (Fig. 3c).

Quantification of apoptosis by FCM. FCM analysis by double staining with Annexin-V (horizontal axis) and PI (vertical axis) demonstrated substantial induction of apoptosis, as depicted in Figure 4a. The incidence of cells in the early apoptotic phase (Annexin-V$^+$, PI$^-$) was 16.3%, and that in late apoptotic phase (Annexin-V$^+$, PI$^+$) was 9.2% after treatment with 0.5% PEG (Fig. 4a right). An approximate 10-fold increase was observed in the percentage of Annexin-V-positive cells (25.5%) with PEG treatment compared to 2.8% for the DMEM-treated control (Fig. 4a left). Furthermore, multinucleated cells demonstrated positive staining for Annexin-V (arrows in Fig. 4b).

In order to clarify whether apoptosis was induced mainly in multinucleated cells, we extracted FCM data sets of only large cells (Fig. 5a), and then replotted the PI signals of each cell against the Annexin-V signals using the above data (Fig. 5b). In Figure 5a, the number of cells in the large-cell fraction (R1), the cut-off value for which was set arbitrarily, increased almost three-fold (8.52 vs 24.26% among 10 000 cells analyzed) after

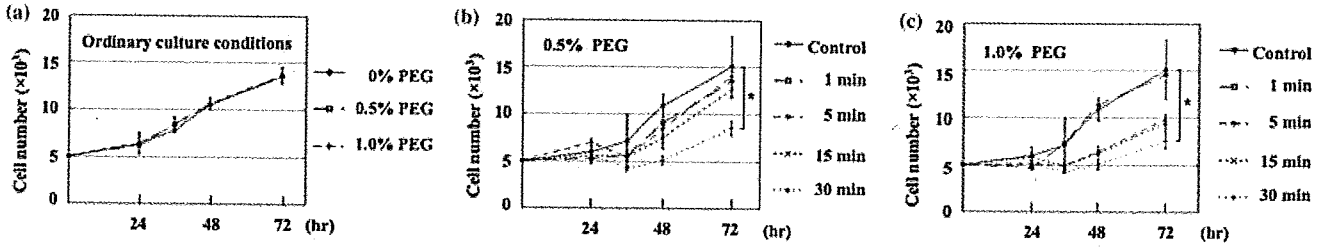

Fig. 2. Polyethylene glycol (PEG) suppresses cell growth at a high cell density. (a) After PEG solution was added into culture media, viable PC-3 cells were counted. (b,c) Following the PEG treatment protocol, PC-3 cells were treated with (b) 0.5% or (c) 1.0% PEG for 1, 5, 15, and 30 min, and viable cells were counted. Values are the mean of fold ± SD. (b) Differences of cell number between 0.5% PEG (30 min) and the Dulbecco's modified Eagle's medium (DMEM)-treated control, and (c) those between 1.0% PEG (30 min) and DMEM-treated control were significant. *$P < 0.05$.

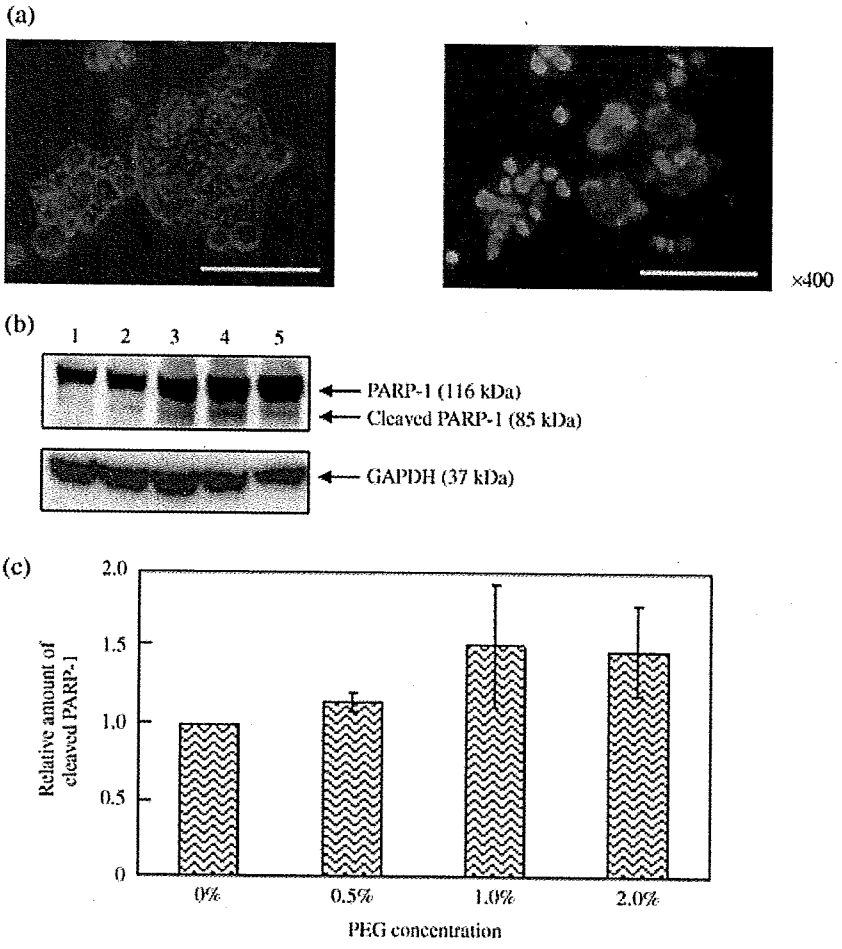

Fig. 3. DNA condensation and poly(ADP-ribose) polymerase (PARP)-1 cleavage. (a) PC-3 cells were treated with 1.0% polyethylene glycol (PEG) for 30 min following the PEG treatment protocol. Cells were stained with Hoechst 33258 (blue), as detailed in Materials and Methods. The left panel indicates the typical morphological feature of multinucleated cell (arrows). The right panel indicates the nuclear condensation of multinucleated cells. Both panels are the same magnification. Scale bars = 50 μm. (b) PARP-cleavage. Whole-cell lysates after treatment with Dulbecco's modified Eagle's medium (DMEM), PEG, or etoposide were prepared, and full-length (uncleaved) PARP-1 (116 kDa), cleaved PARP-1 (85 kDa), and glyceraldehyde-3-phosphate dehydrogenase (GAPDH) (37 kDa) were immunoblotted. Lane 1, DMEM; lane 2, 0.5% PEG; lane 3, 1.0% PEG; lane 4, 2.0% PEG; lane 5, etoposide (positive control). (c) Quantification of the cleaved PARP-1 protein by western blot analysis. The density of both non-cleaved and cleaved PARP-1 and of the background levels were measured, and the ratios of cleaved PARP-1 against the total PARP-1 were calculated as follows: (density of cleaved PARP-1) – (background level)/(density of total PARP-1) – (background level).

0.5% PEG treatment. In Figure 5b, among the cells in the R1 fraction, 292 and 1571 cells in DMEM-treated control and 0.5% PEG-treated group respectively, showed positive for Annexin V. Namely, an approximate five-fold increase in apoptotic cells was observed within the large-cell fraction of PEG-treated cells compared to DMEM-treated cells. In particular, a more than 20-fold increase was observed in the number of cells in early apoptotic phase (25 vs 656 cells). Similar results were obtained with various cut-off values for R1 to include 3.0% and 5.5% of total populations in DMEM-treated cells (data not shown).

No evidence of mitotic catastrophe in PEG-treated cells. By FCM analysis, no marked changes in cell cycle profile were apparent after PEG treatment (Fig. 6a). Although the number of cells in the sub-G_1 fraction was slightly increased by PEG treatment, cells in the G_1, S, G_2/M, and > G_2/M fractions were not changed significantly (Fig. 6b). We also noted that the number of cells in > G_2/M fractions decreased substantially between 34 and 36 h after PEG treatment, as depicted in Supplemental Fig. 1.

We then extracted aneuploid-cell and large-cell populations from the > G_2/M fraction using the FCM data set, as detailed in Supplemental Fig. 2A, and the corresponding number of cells in Supplemental Fig. 2A was counted between 34 and 36 h (Supplemental Fig. 2B). The number of aneuploid cells in the > G_2/M fraction did not show a significant change between 34 and 36 h after 0.5 and 1.0% PEG treatment. However, an approximate 20% increase in the numbers of large cells in the > G_2/M fraction was observed 34 h after PEG treatment, which substantially decreased at 36 h (Supplemental Fig. 2B). These results further

doi: 10.1111/j.1349-7006.2008.00781.x

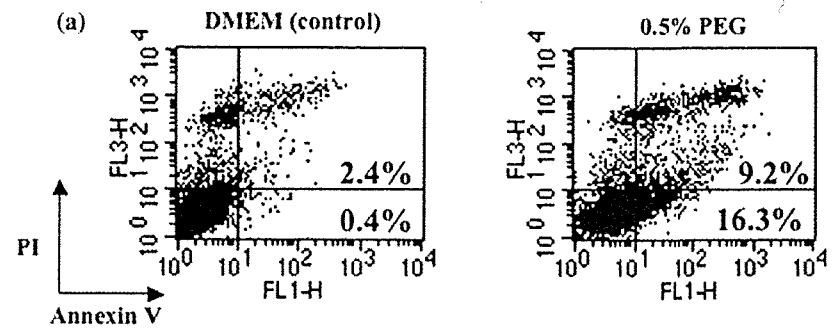

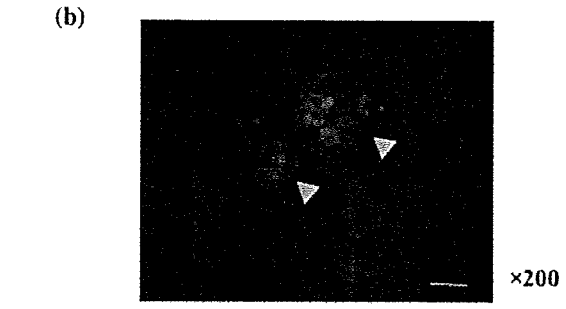

Fig. 4. Quantification of apoptosis using flow cytometry (FCM). (a) PC-3 cells were treated with Dulbecco's modified Eagle's medium (DMEM) alone (left) or 0.5% polyethylene glycol (PEG) (right) for 1 min following the PEG treatment protocol. After double-staining with Annexin-V and propidium iodide (PI), apoptotic cells were analyzed by FCM. (b) Multinucleated giant cells (arrow) visualized by staining with Annexin-V (green) and PI (red). Scale bar = 50 μm.

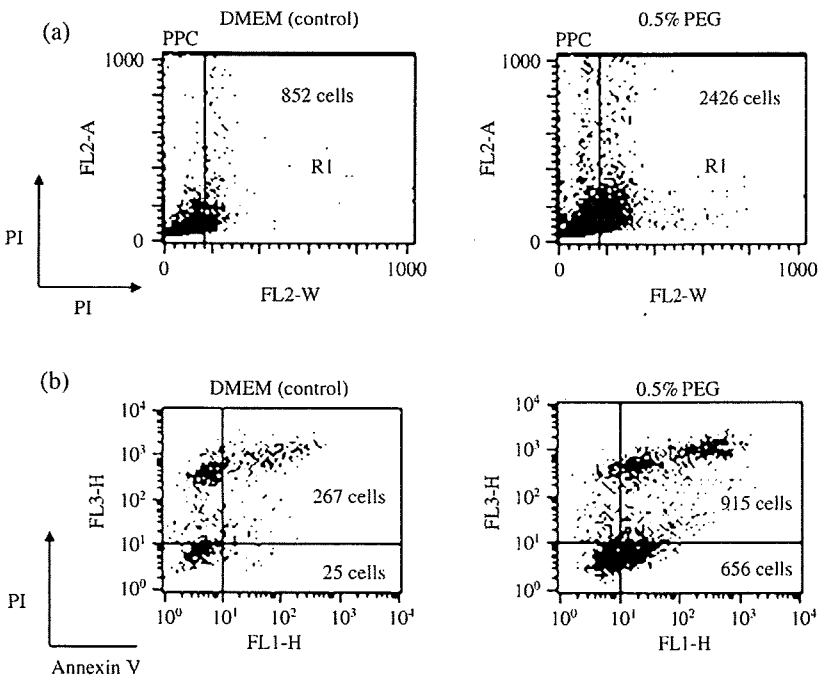

Fig. 5. Induction of apoptosis in large cells induced by polyethylene glycol (PEG) treatment. (a) From the data sets presented in Figure 4a, large cell populations were examined. (b) On the data sets presented in (a), the large cells gating the R1 region were replotted by propidium iodide (PI) signals against Annexin-V.

support the view that reduction of cell numbers by PEG treatment occurs in large-cell fractions, possibly by apoptosis, but not by mitotic catastrophe in aneuploid cells.

Induction of apoptosis by PEG in PC-3 xenografts. Following the PEG treatment protocol, PC-3 cells were pretreated with DMEM or 0.5% PEG and then implanted into mice. At day 7, the tumor volume of the PEG-treated group was significantly reduced compared to the DMEM-treated group. An approximate 50% reduction in tumor volume was observed with PEG treatment (Fig. 7a). To further confirm the growth-suppressive effect of PEG in an *in vivo* setting, we conducted the following experiment. Non-treated PC-3 cells were implanted into mice, and PBS or 0.5% PEG solution was injected into palpable tumors from day 7, twice a week (Fig. 7b top). The volumes of PC-3 xenografts increased approximately eight-fold from day 7 to day 25 in the PBS-injected group (Fig. 7b bottom). In contrast, substantial suppression of tumor growth was detected after injecting 0.5% PEG solution directly into tumors. The average sizes of tumors in PBS- and 0.5% PEG-injected groups at day 25 were 1344 ± 292 and 812 ± 215 mm^3, respectively. Namely, tumor volumes were reduced approximately 30% in the PEG-injected group compared with those in the PBS group at